



Universiteit
Leiden
The Netherlands

Keratin 8 is a scaffolding and regulatory protein of ERAD complexes

Pranke, I.M.; Chevalier, B.; Premchandrar, A.; Baatallah, N.; Tomaszewski, K.F.; Bitam, S.; ... ; Edelman, A.

Citation

Pranke, I. M., Chevalier, B., Premchandrar, A., Baatallah, N., Tomaszewski, K. F., Bitam, S., ... Edelman, A. (2022). Keratin 8 is a scaffolding and regulatory protein of ERAD complexes. *Cellular And Molecular Life Sciences*, 79(9). doi:10.1007/s00018-022-04528-3

Version: Publisher's Version

License: [Leiden University Non-exclusive license](#)

Downloaded from: <https://hdl.handle.net/1887/3564847>

Note: To cite this publication please use the final published version (if applicable).



Keratin 8 is a scaffolding and regulatory protein of ERAD complexes

Iwona Maria Pranke¹ · Benoit Chevalier¹ · Aiswarya Premchandrar³ · Nesrine Baatallah¹ · Kamil F. Tomaszewski¹ · Sara Bitam¹ · Danielle Tondelier¹ · Anita Golec¹ · Jan Stolk⁴ · Gergely L. Lukacs^{5,6} · Pieter S. Hiemstra⁴ · Michal Dadlez³ · David A. Lomas⁷ · James A. Irving⁷ · Agnes Delaunay-Moisan⁸ · Eelco van Anken⁹ · Alexandre Hinzpeter¹ · Isabelle Sermet-Gaudelus^{1,2} · Aleksander Edelman¹

Received: 7 February 2022 / Revised: 8 August 2022 / Accepted: 12 August 2022 / Published online: 1 September 2022
© The Author(s), under exclusive licence to Springer Nature Switzerland AG 2022

Abstract

Early recognition and enhanced degradation of misfolded proteins by the endoplasmic reticulum (ER) quality control and ER-associated degradation (ERAD) cause defective protein secretion and membrane targeting, as exemplified for Z-alpha-1-antitrypsin (Z-A1AT), responsible for alpha-1-antitrypsin deficiency (A1ATD) and F508del-CFTR (cystic fibrosis transmembrane conductance regulator) responsible for cystic fibrosis (CF). Prompted by our previous observation that decreasing Keratin 8 (K8) expression increased trafficking of F508del-CFTR to the plasma membrane, we investigated whether K8 impacts trafficking of soluble misfolded Z-A1AT protein. The subsequent goal of this study was to elucidate the mechanism underlying the K8-dependent regulation of protein trafficking, focusing on the ERAD pathway. The results show that diminishing K8 concentration in HeLa cells enhances secretion of both Z-A1AT and wild-type (WT) A1AT with a 13-fold and fourfold increase, respectively. K8 down-regulation triggers ER failure and cellular apoptosis when ER stress is jointly elicited by conditional expression of the μ_s heavy chains, as previously shown for Hrd1 knock-out. Simultaneous K8 silencing and Hrd1 knock-out did not show any synergistic effect, consistent with K8 acting in the Hrd1-governed ERAD step. Fractionation and co-immunoprecipitation experiments reveal that K8 is recruited to ERAD complexes containing Derlin2, Sel1 and Hrd1 proteins upon expression of Z/WT-A1AT and F508del-CFTR. Treatment of the cells with c407, a small molecule inhibiting K8 interaction, decreases K8 and Derlin2 recruitment to high-order ERAD complexes. This was associated with increased Z-A1AT secretion in both HeLa and Z-homozygous A1ATD patients' respiratory cells. Overall, we provide evidence that K8 acts as an ERAD modulator. It may play a scaffolding protein role for early-stage ERAD complexes, regulating Hrd1-governed retrotranslocation initiation/ubiquitination processes. Targeting K8-containing ERAD complexes is an attractive strategy for the pharmacotherapy of A1ATD.

Keywords Intermediary filaments · Cytoskeleton · Protein–protein interaction · Protein complexes fractionation · Synthetic lethality · Epithelium

Introduction

Proper protein folding represents one of the primary challenges for cells to maintain proteostasis. This complex process is challenged by the intrinsic properties of proteins or

mutations in protein-coding genes. Proteins entering the secretion pathway that fail to fold, assemble or post-translationally mature properly are eliminated by ERAD. ERAD relies on multiple dynamic protein complexes acting sequentially to recognize, tether, ubiquitin-tag and extract misfolded substrates from the ER, thereby enabling their proteasomal degradation in the cytosol [6, 35, 48]. Distinct ERAD pathways accommodate the variety of topologies and post-translational modifications encountered in misfolded protein substrates. The partial redundancy of ERAD factors allows cells to oversee proteostatic stress and maintain ER homeostasis coordinately. ERAD pathways can be divided into the following functional modules: (i) substrate recognition; (ii)

Benoit Chevalier, Aiswarya Premchandrar, Alexandre Hinzpeter, Isabelle Sermet-Gaudelus have equally participated.

✉ Iwona Maria Pranke
iwona.pranke@inserm.fr

✉ Aleksander Edelman
aleksander.edelman@inserm.fr

Extended author information available on the last page of the article

retrotranslocation initiation with substrate unfolding involving mainly multifunctional Derlin proteins; (iii) ubiquitination of the partially dislocated substrate, assisted by different membrane-bound E3 ubiquitin ligases (e.g., a multimeric complex, containing Hrd1 E3 ligase coupled to substrate recognition protein Sel1) and associated ubiquitin-conjugating enzymes E2s according to substrates [2, 53, 61]; therefore licensing; (iv) the dislocation process ensured by p97/VCP ATPase providing a pulling force [17, 36, 45]; and finally (v) substrate degradation by 26S proteasome.

Protein misfolding underlies two frequent pulmonary genetic diseases, A1ATD and CF. The most common disease-causing protein folding mutations are Glu342Lys (Z) in A1AT and F508del in CFTR [18, 24, 54]. Over 99% of F508del-CFTR and ~70% Z-A1AT are degraded by ERAD [22, 28, 55]. Both misfolded proteins form complexes with ER chaperones (e.g., Calnexin) [27, 50], ubiquitin ligases (e.g., Hrd1 and its partner Sel1) [19, 20, 25, 32, 52], and dislocating protein p97/VCP [4, 26, 41]. Consequently, misfolded F508del-CFTR is less efficiently targeted to the apical membrane (PM) of epithelial cells and secretion of misfolded Z-A1AT is strongly decreased (to ~10–15% of WT level). In addition, the folding efficacy of WT-CFTR is limited as observed in heterologous overexpressing system, but not clearly confirmed in native tissue [39, 40], and the thermodynamic state of WT-A1AT is suboptimal [5], both features favoring ERAD degradation of the WT isoforms [60]. Additionally, for Z-A1AT, which is highly expressed in the hepatocyte, its accumulation in the ER also activates classic autophagy [28] and ER-to-lysosome-associated degradation [16].

An increasing body of evidence suggests that K8 and Keratin 18 (K18), proteins forming intermediary filament (IF) heterodimers in simple epithelia [21], can regulate protein targeting to the apical plasma membrane [8, 34, 56]. They also display additional roles beyond mechanical and structural functions, including protein polyubiquitination in a pro-inflammatory context [12] or Akt-signaling regulation [31]. Our previous studies [7, 11] revealed that K8 and K18 regulate F508del-CFTR trafficking. We have determined that K8 favored F508del-CFTR retention in the ER [7], an effect that can be alleviated pharmacologically with small molecules, e.g., c407 [38], and/or reducing K8 concentrations by siRNA [7].

Here, we show that K8 regulates the secretion of Z-A1AT. Since K8 affects the targeting of two ERAD substrates, Z-A1AT and F508del-CFTR, we challenged the hypothesis that K8 is part of the ERAD pathway. We gathered genetic and biochemical clues pointing to a new physiological function of K8 during the ERAD process. As for significant ERAD components (Hrd1, Sel1) [62] in conditions triggering ER stress, we observed that K8 is essential to prevent ER failure and associated cell death. K8 co-sedimented and

co-precipitated with major ERAD components (Derlin2, Hrd1 and Sel1), consistent with K8 acting as a scaffold in the Hrd1-dependent ERAD pathway. Finally, we provide proof of concept that modulation of K8-containing ERAD complexes increases Z-A1AT secretion from HeLa, and patients derived primary human respiratory epithelial (HNE) cells and could be a target for pharmacotherapy in A1ATD.

Results

Silencing K8 expression increases WT-A1AT and Z-A1AT secretion through the conventional secretory pathway

The implication of K8 in the secretion of WT-A1AT and misfolded Z-A1AT was evaluated in HeLa cells upon reduced K8 levels (shRNAK8, see Material and Methods section) (Fig. 1A, B). Quantification of A1AT in the supernatants of control and shK8 cells showed significantly enhanced secretion of both Z-A1AT and WT-A1AT in shK8 cells (Fig. 1B, lane numbers 1 and 2 for both A1AT WT and Z), with a 13-fold and fourfold increase of secretion, respectively (Fig. 1B lane numbers 1 and 2 for both A1AT WT and Z). This secretion was associated with an increased intracellular pool of Z-A1AT (Fig. 1C, D, lane numbers 1 and 2), suggesting its stabilization.

The enhanced WT- and Z-A1AT secreted by shK8 cells had an identical SDS-gel migration pattern compared to WT- and Z-A1AT secreted by control cells (Fig. 1A, lane number 1 vs. 2 for both A1AT WT and Z, shRNAK8- vs. shRNAK8+), indicative of a similar glycosylation pattern and secretion occurring through the conventional secretory pathway. This was confirmed using Brefeldin A (BFA), an inhibitor of the conventional secretory pathway, which abolished WT-/Z-A1AT secretion from both control and shK8 cells (Fig. 1A, B). Upon BFA treatment, an increase of Z- and WT-A1AT intracellular concentrations was observed in shK8 cells compared to control cells (Fig. 1C, D), consistent with reduced degradation of WT-/Z-A1AT upon decreased K8 expression.

To determine if the observed increase in WT-/Z-A1AT secretion was not linked to a general effect on proteins secretion, we performed several series of control experiments: (i) quantification of the secretome protein content did not differ in shK8 and K8-expressing (control) HeLa cells (Supp. Fig. 2A); (ii) secretion of transfected *Gaussia* luciferase was not modified (Supp. Fig. 2B); (iii) secretion of ER protein, BiP, both from control and shRNA K8 cells was not detectable by Western blot (Supp. Fig. 2C); (iv) expression of endogenous Na⁺K⁺ATPase at the plasma membrane was not changed upon K8 silencing (Supp. Fig. 2D); (v) secretion of heavy chain subunit μ_s of secretory IgM from control

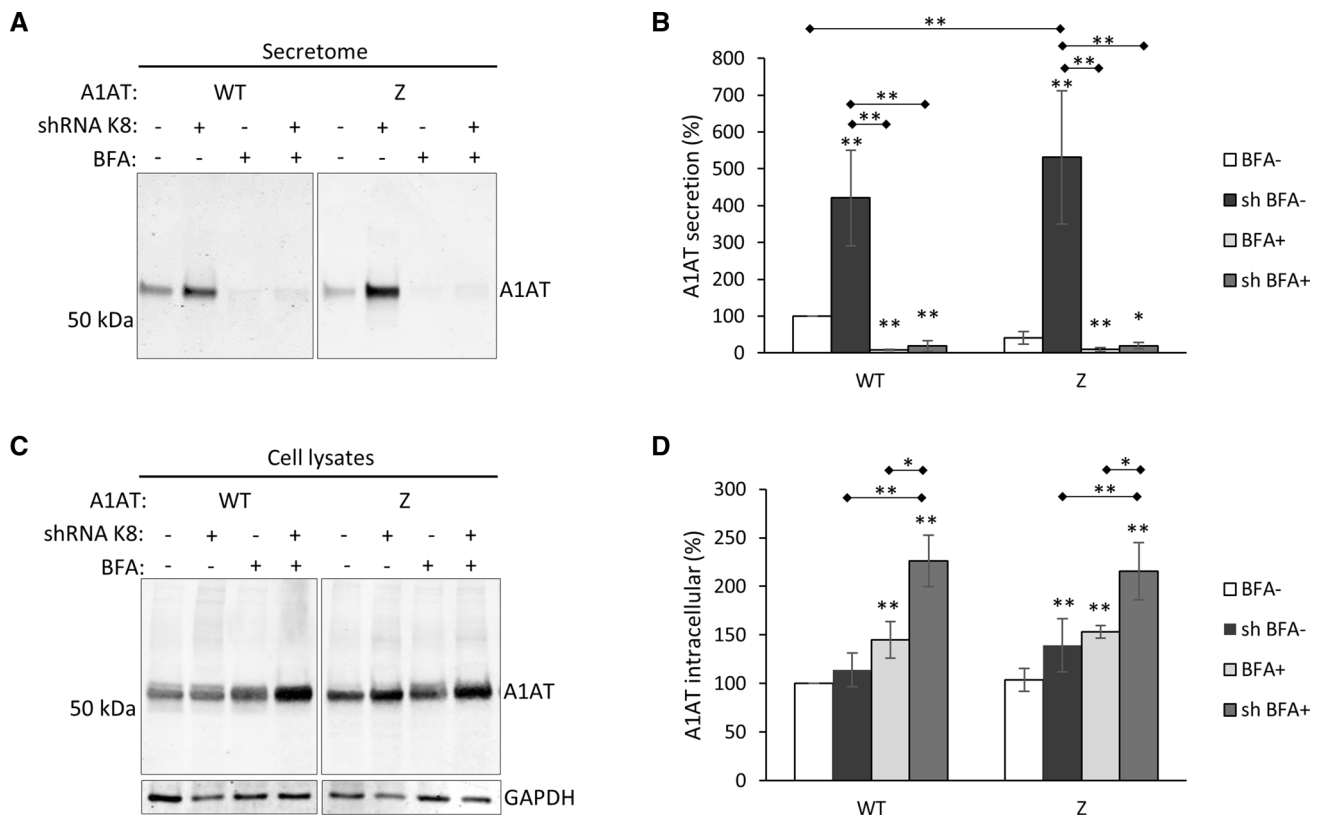


Fig. 1 Silencing K8 in HeLa cells increases the secretion of Z-A1AT and WT-A1AT through conventional secretory pathway. **A** WB analysis of secretion of WT-A1AT/Z-A1AT in cell cultures with normal (shRNAK8-) and decreased (shRNAK8+) level of K8 expression after treatment with Brefeldin A 5 μ g/ml (BFA+) or vehicle (BFA-) for 7 h. Representative image and quantification from $n=9$ independent experiments. **B** Quantification of secretion (mean \pm SD) normalized to total protein concentrations in respective cell lysates from at least four experiments. * <0.05 ; ** <0.005 ; *** <0.0005 (Mann-Whitney test); *over the bar indicates p value vs. control (white

boxes), if otherwise it is indicated. **C** WB analysis of intracellular WT-A1AT/Z-A1AT in cell cultures with normal (shRNAK8-) and decreased (shRNAK8+) level of K8 expression after treatment with Brefeldin A 5 μ g/ml (BFA+) or vehicle (BFA-) for 7 h. Representative image and quantification from $n=9$ independent experiments. **D** Quantification of secretion (mean \pm SD) normalized to total protein concentrations in respective cell lysates from at least 4 experiments. * <0.05 ; ** <0.005 ; *** <0.0005 (Mann-Whitney test); * over the bar indicates p value vs. control (white boxes), if otherwise it is indicated

and shRNA K8 cells was not detectable (Supp. Fig. 2E); and (vi) there was no change in ER and secretory proteins in the secretome of shRNA K8 cells compared to control cells (Supp. Fig. 2F). Altogether these experiments suggest that K8-dependent regulation of secretion was specific of misfolded Z-A1AT or unstable WT-A1AT.

The accumulation of Z-A1AT upon BFA treatment in shK8 cells suggests an implication of K8 in the degradation via the ERAD or the autophagy pathways [28]. To test for a possible role of K8 silencing in rescuing Z-A1AT from autophagy, the effect of Wortmannin (1 μ M, 24 h), an inhibitor of phosphoinositide 3-kinases, was tested. Intracellular accumulation of non-mature Z-A1AT upon treatment was observed without increased secretion (Supp. Fig. 3A). Autophagy induction by MK-2206 (5 μ M, 20 h), an inhibitor of Akt-signaling pathway, did not increase A1AT secretion from both normal and shRNAK8 cells (Supp. Fig. 3B). Thus, the increase of A1AT secretion upon K8 silencing

does not result from the autophagy pathway. On the other hand, a slightly increased expression of Grp78/BiP was observed (Supp. Fig. 3C) in shK8 cells, supporting a potential implication of K8 in the ERAD pathway. This is not due to the ER stress as another marker of ER stress, CHOP, was not changed (Supp. Fig. 3C) suggesting that BiP increase may be linked to K8 silencing which potentially influences the ER processes.

K8 is a critical factor for ERAD of μ_s

To evaluate the potential role of K8 in ERAD, we took advantage of a cellular model system expressing the heavy chain μ_s subunit of secretory IgM. There, the lethal accumulation of μ_s in the ER due to the absence of the light chain to enable antibody reconstitution and secretion is counterbalanced by enhanced ERAD degradation. The implication of K8 in the degradation of μ_s was monitored via cell death

upon K8 silencing (synthetic lethality assay or growth assay, see Methods section for details).

K8 silencing triggered synthetic lethality of μ_s -expressing cells (Fig. 2A; siK8 + μ_s). None of the other conditions (siRNA against K8 alone (siK8- μ_s)) and μ_s

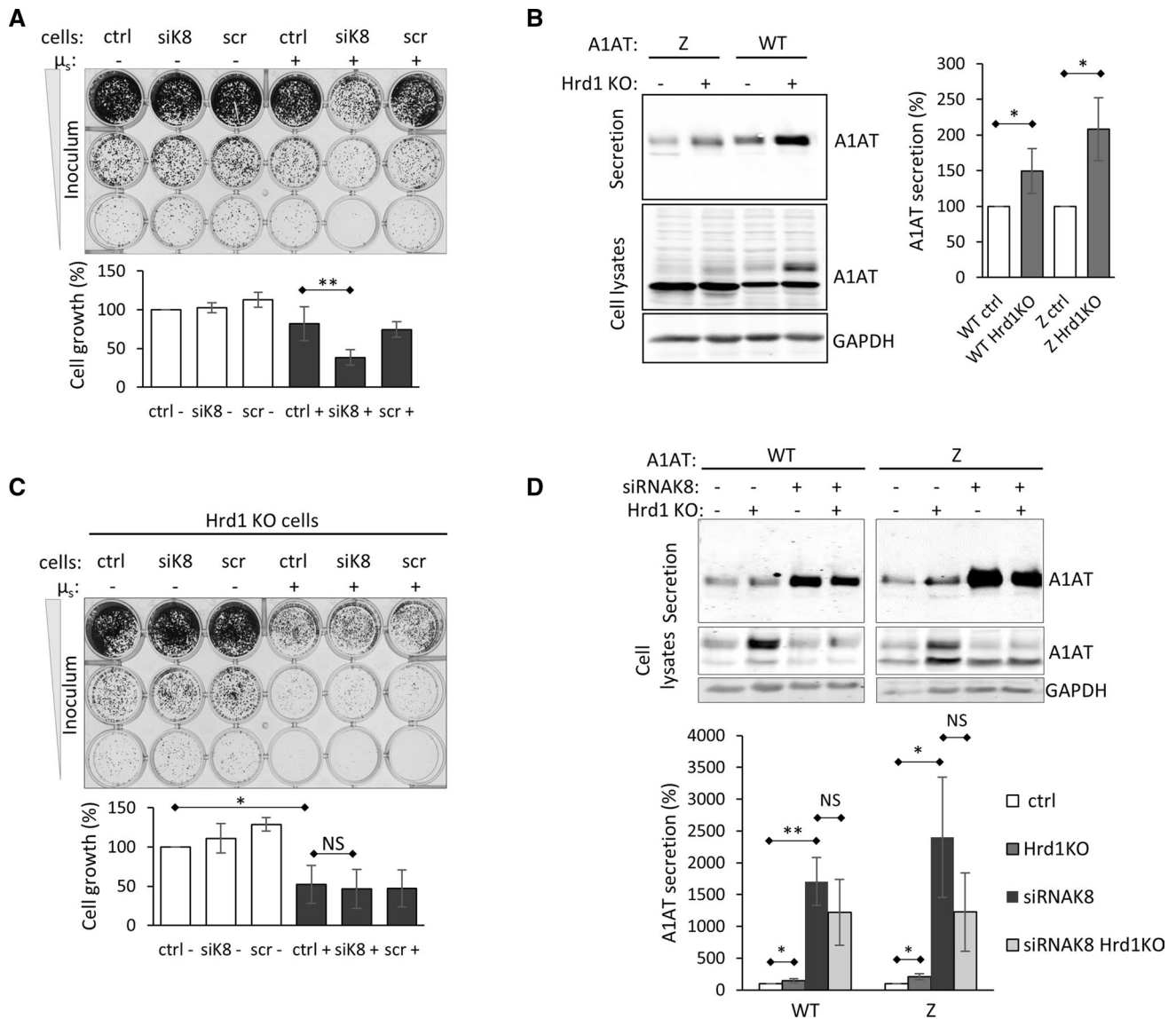


Fig. 2 K8 regulates Hrd1-dependent processes. **A** Synthetic lethality of HeLa cells conditionally expressing μ_s . Cells transfected with siRNA against K8 (cells siK8), or scrambled siRNA (cells scr) were treated with 0.5 nM Mifepristone (Mif) (μ_s +) or vehicle (μ_s -). After transfection cells were seeded upon 1:5 serial dilution (inoculum 5000, 1000, 200 cells) into 24-well plates and grown for 7 days. Scrambled RNA had no effect on cell growth of non-expressing (scr- μ_s) and μ_s -expressing cells (scr+ μ_s). This is a representative image of a culture plate and quantification of cell growth (inoculum 1000 cells, middle row) as mean % (\pm SD) of growth in non-transfected non-treated cells (ctrl-) of five independent experiments are shown. $^{**}p < 0.005$ (paired *t* test). **B** Effect of Hrd1 knock-out on WT-A1AT and Z-A1AT secretion from HeLa cells. WB images show WT-A1AT and Z-A1AT secretion levels (upper panel), A1AT expression (middle panel) and GAPDH as loading control (lower panel). Protein quantification is expressed as means \pm SD from four inde-

pendent experiments. $^{*}p < 0.05$ (Mann-Whitney test). **C** Synthetic lethality of Hrd1KO HeLa cells. Cells were treated as in (A). Representative image of culture plate and quantification of cell growth (inoculum 1000 cells, middle row) as mean % (\pm SD) of growth in non-transfected non-treated cells (ctrl-) of five independent experiments are shown. $^{*}p < 0.05$ (paired *t* test). **D** Effects of K8 silencing, Hrd1 knock-out and their combination on secretion of WT-A1AT and Z-A1AT. Normal (Hrd1KO-) and Hrd1KO (Hrd1KO+) HeLa cells were transiently transfected with WT-A1AT or Z-A1AT and with siRNA against K8 (siRNAK8+). Representative WB images demonstrating WT-A1AT and Z-A1AT secretion (upper image), WT-A1AT and Z-A1AT expression (middle image) and GAPDH (bottom image) from normal, Hrd1KO+, siRNAK8+ and siRNAK8+/Hrd1KO+ HeLa cells. Protein quantification of A1AT secretion is expressed as mean \pm SD for three experiments. $^{*}p < 0.05$, $^{**}p < 0.005$ (Mann-Whitney test)

expression alone (ctrl + μ_s) led to significant cell death, asserting the features of *bona fide* synthetic lethality (Fig. 2A). These results showed that decreasing K8 levels in μ_s -expressing cells led to their decreased viability, probably by compromising the ERAD pathway and overload of ER with μ_s .

K8 regulates Hrd1-dependent processes

We then searched for the ERAD process affected by K8 silencing. It has been previously shown that misfolded Z-A1AT secretion is not increased by inhibiting the proteasome [55]. We, thus, focused on ERAD steps governed by Hrd1 and p97/VCP (Supp. Fig. 1, Modules 2B and 3).

Knocking out Hrd1 in HeLa cells (stable Hrd1KO HeLa cells) [62] increased Z-A1AT and WT-A1AT secretion (Fig. 2B), as already shown by Joly et al. [23] for Z-A1AT. It was accompanied by increased levels of fully glycosylated Z- and WT-A1AT in Hrd1KO cells (Fig. 2B). Therefore, disruption of the Hrd1 complex and consequently inhibition of substrate ubiquitination/retrotranslocation (Supp. Fig. 1, module 2A and 2B) appears to be an essential step favoring both WT-A1AT and Z-A1AT secretion.

To further investigate this question, we examined whether K8 is involved in the ERAD processes controlled by Hrd1. The effect of combining Hrd1KO and siRNAK8 was evaluated using synthetic lethality and A1AT secretion assays. Hrd1KO cells showed a significant synthetic lethality of cells upon μ_s induction (ctrl, siRNAK8, and scramble), underlining the importance of Hrd1 (Fig. 2C). When combining Hrd1KO and siRNAK8, no additive or synergistic effect was observed in synthetic lethality (Fig. 2C) or increased WT-/Z-A1AT secretion (Fig. 2D). The effect of K8 KD was stronger (Fig. 2D) suggesting potential regulation of multiple proteins of the ERAD complex. Both growth and secretion assays showed that Hrd1 and K8 modulate the secretion of WT-/Z-A1AT via the same pathway.

Pharmacological inhibition of VCP/p97 protein with Eeyarestatin I or NMS-873 was performed to test for the role of substrate dislocation (Supp. Fig. 1, module 3) on WT-/Z-A1AT secretion (Supp. Fig. 4A, B). Both inhibitors led to the intracellular accumulation of Z-A1AT and WT-A1AT, consistent with reduced degradation. Nonetheless, this was not associated with increased WT-/Z-A1AT secretion (Supp. Fig. 4A, B, Secretion panels and quantification), indicating that the inhibition of substrate dislocation was insufficient to enhance secretion.

The observations above emphasized (i) the relationship between K8 and Hrd1 and (ii) the absence of increased secretion upon p97 inhibition, suggesting that K8 modulates early ERAD processes, i.e., Hrd1-dependent ubiquitination and initiation of retrotranslocation (Supp. Fig. 1).

K8 is recruited to ERAD complexes

For further insight into the involvement of K8 into ERAD processes, we determined if K8 is recruited to the ERAD complexes by performing sucrose gradient fractionations of ERAD complexes. The distribution of K8 and three important proteins of the Hrd1 complex (Hrd1, Sel1 and Derlin2; Supp. Fig. 1, modules 2A and B) was monitored in mock-transfected cells and cells expressing WT-, Z-A1AT or μ_s .

In mock-transfected cells, K8 was primarily associated with lower sedimentation fractions (3–6) together with Derlin2 and a smaller amount of Sel1 (Fig. 3A–C). This suggested that K8 forms complexes, at the least, with Derlin2 and Sel1 (Fig. 7).

Expression of either Z-A1AT, μ_s , or WT-A1AT, shifted K8 (Fig. 3A) together with Derlin2, Sel1 and Hrd1 (Fig. 3B–D) toward heavier fractions compared to mock-transfected cells. This is consistent with the dynamic recruitment of K8 to different higher-order ERAD complexes upon expression of an ERAD substrate (Fig. 7). The observed differences in the distribution of WT-A1AT, Z-A1AT and μ_s proteins in sucrose gradients may be due to the differences in the recruitment of these proteins to degradation processes (Fig. 3E).

The existence of ERAD complexes including K8 was further validated by co-immunoprecipitation experiments performed in both polarized primary HNE cells endogenously expressing Z-A1AT (Fig. 3F) and HeLa cells transfected with WT or Z-A1AT (Supp. Fig. 4C). Derlin2, Hrd1 and Sel1 proteins were detected in immuno-precipitates of K8 and conversely K8, Hrd1 and Sel1 were co-immunoprecipitated with Derlin2.

To test if K8 influenced the formation of the ERAD complexes, we performed fractionation experiments on proteins obtained from shK8 mock- and shK8 Z-A1AT-transfected cells (Fig. 4). Under shK8 conditions, the total residual K8 co-sedimented with Derlin2 to one low-density fraction, unmasking a possible Derlin2-K8 complex (Fig. 4A, B, shK8 lines for K8 and Derlin2, black arrows). Profiles of Hrd1 and Sel1 fractionation were similar in mock-transfected and shK8 cells (Fig. 4C, D, compare lines shK8 and mock for Hrd1 and Sel1), suggesting that K8 does not influence the formation of complexes with Hrd1 and Sel1 under these conditions. The importance of K8 for the recruitment of Hrd1 and Sel1 to higher density complexes appeared on fractionation profiles of proteins derived from Z-A1AT expressing cells with normal and decreased levels of K8 (Fig. 4C, D). Noteworthy was that Hrd1 and Sel1 amounts were reduced in fraction 12 of the shK8 Z-A1AT sedimentation profile compared to cells expressing normal levels of K8 (Fig. 4C, D, red boxes). This shows that K8 favored the recruitment of Hrd1 and Sel1 to high-order complexes under the expression of Z-A1AT.

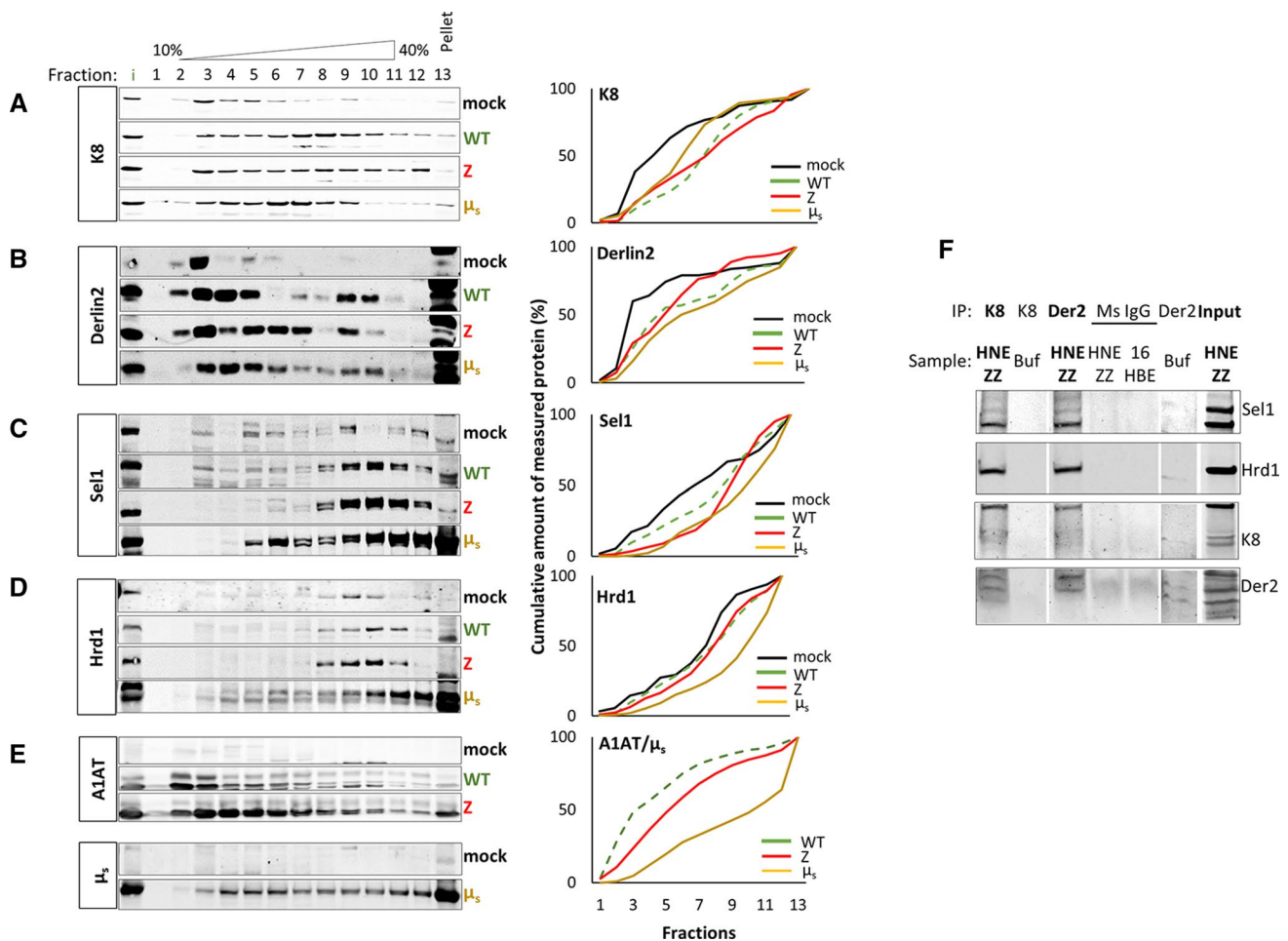


Fig. 3 K8 is recruited to the ERAD complexes upon overexpression of misfolded Z-A1AT, WT-A1AT and μ_s . Sucrose gradient fractionation of the ERAD complexes. HeLa cells expressing WT-A1AT (WT-A1AT), Z-A1AT (Z-A1AT), μ_s (Mif 0.5 nM for 24 h) (μ_s), or mock-transfected (mock). Protein samples from cells were sedimented over a 10–40% sucrose gradient. K8 (A), Sel1 (B), Hrd1 (C), Derlin-2 (D), and μ_s /WT-A1AT/Z-A1AT (E) were detected by immunoblotting with respective antibodies and semi-quantified (right panels). Quantifications represent results shown in the corresponding images on the left and are expressed as cumulative amount of measured protein (%) to demonstrate the overall shift. In the right panel: black lines correspond to protein content in low density ERAD complexes under basal conditions, green, red, and yellow lines show ERAD complexes formed upon WT-A1AT, Z-A1AT and μ_s expression, respectively.

Co-staining of K8 and Calnexin (CNX) showed a redistribution of K8 to the vicinity of the ER in Z-A1AT-expressing cells vs. WT-A1AT and mock-transfected cells (Supp. Fig. 5A). K8 co-distributed with Z-A1AT in HeLa and primary HBE cells as shown by immunocytochemistry (Supp. Fig. 5B, C) and proximity ligation assay (Supp. Fig. 6A, B). K18 also co-distributed with WT and Z-1AT but without the increased proximity to Z-A1AT, in contrast to what was observed for K8 (Supp. Fig. 6C). Subcellular fractionation (Supp. Fig. 6D) showed that K8 association with

The three tested substrates distributed differently in sucrose gradients: a large amount of μ_s which is a substrate efficiently processed by ERAD strongly distributed to heavy fractions, a relatively large amount of Z-A1AT distributed to heavy fractions, whereas smaller amounts of WT-A1AT were recruited to heavy fractions. Experiments were performed at least three times for all tested conditions. **F** Co-immunoprecipitation of ERAD complexes from microsomes of polarized primary human nasal epithelial cells homozygous for Z mutation of A1AT. Derlin2 or K8 were immunoprecipitated with anti-Derlin2 or anti-K8 antibodies, respectively (see Methods section) and proteins of interest were detected using corresponding antibodies (Sel1, Hrd1, K8, Derlin2). Negative controls with unspecific mouse IgG (Ms IgG) and extracts, as well as with anti-Derlin2/K8 antibody and LMNG buffer were applied

ER-containing microsomes (attested by the presence of Calreticulin, Supp. Fig. 6E) was enriched in Z-A1AT-expressing cells. Finally, Proteinase K assay experiments [3] excluded intra-ER localization of K8 (Supp. Fig. 6E) as it was fully digested in both the presence and absence of detergent, a feature consistent with the reported cytosolic localisation of K8 (according to Human Protein Atlas and [9]). Altogether, these observations are consistent with sucrose gradient fractionation results described above and support the implication of K8 in the degradation processes within ERAD.

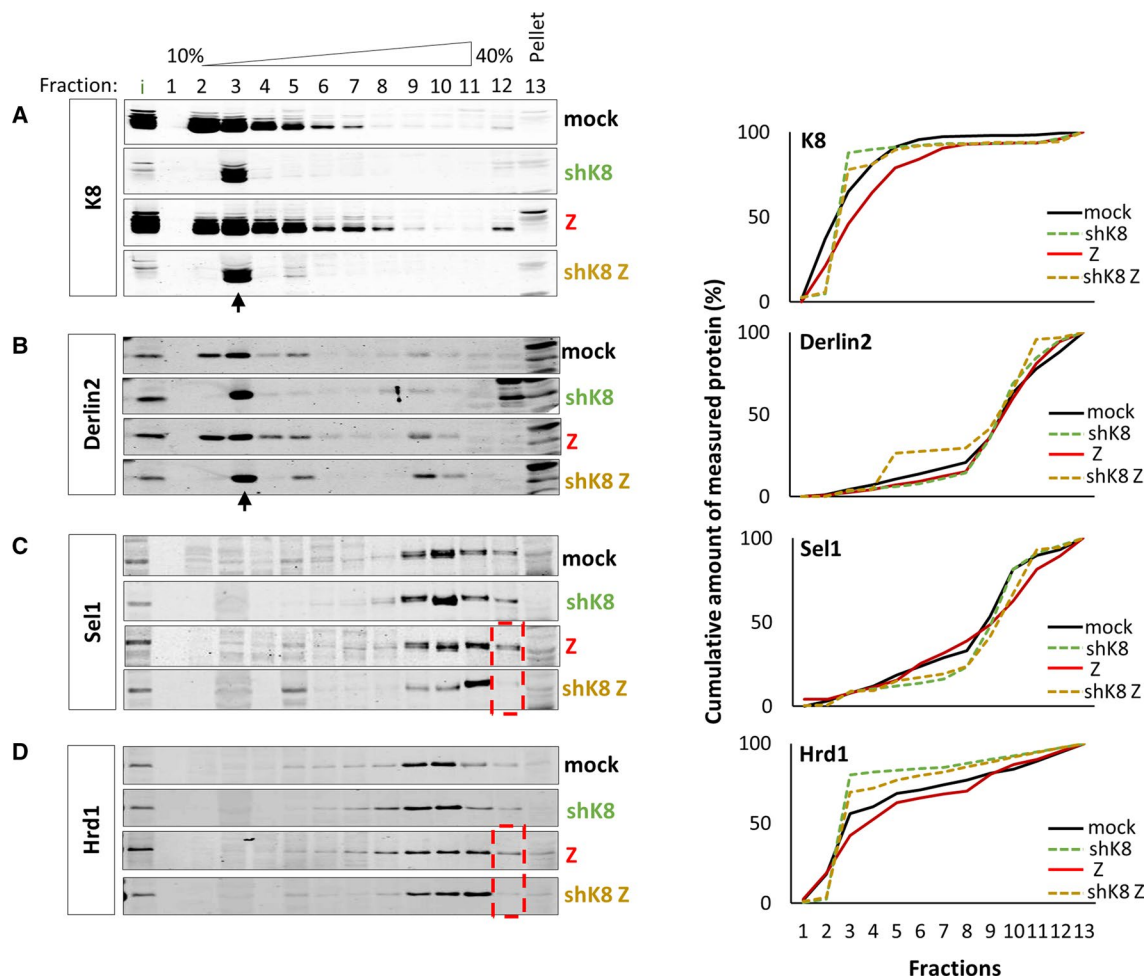


Fig. 4 Silencing K8 affects ERAD complexes formation. Sucrose gradient fractionation of the ERAD complexes. HeLa cells expressing normal (mock and Z-A1AT) and decreased level of K8 (shK8 and shK8 Z-A1AT). Protein samples from cells were sedimented over a 10–40% sucrose gradient. K8 (**A**), Sel1 (**B**), Hrd1 (**C**), Derlin-2 (**D**) were detected by immunoblotting with respective antibodies. Black arrows correspond to ERAD complexes containing K8 and Derlin2

formed in shK8 cells, red dashed lined boxes correspond to high-density ERAD complexes formed in presence of K8 and Z-A1AT (Z-A1AT cells) but missing in shK8 Z-A1AT cells. Quantifications represent results shown in the corresponding images on the left and are expressed as cumulative amount of measured protein (%) to demonstrate the overall shift

To test whether other misfolded proteins recruited K8 to ERAD complexes, we conducted sucrose gradient fractionations of samples from WT-CFTR and F508del-CFTR-expressing 16HBE14o-cells. Analysis of protein complexes (Fig. 5) showed that Derlin2, Hrd1 and K8 shifted towards heavier fractions (Fig. 5A–D) upon F508del-CFTR expression compared to WT-CFTR, similar to that observed for Z-A1AT and μ_s (Fig. 3A, B and D). Noticeably, the Sel1 shift to heavier fractions was weaker on F508del-CFTR than Z-A1AT, WT-A1AT and μ_s . The less pronounced shift of Sel1 towards high-density fractions upon F508del-CFTR expression could be explained because F508del-CFTR is expressed at an endogenous level compared to transiently transfected Z-A1AT. Recruitment of K8 to ERAD complexes was supported by co-immunoprecipitation of K8 with

Derlin2 and Hrd1 from lysates of 16HBE cells expressing WT or F508del-CFTR (Fig. 5E).

Altogether, the results obtained for misfolded Z-A1AT and F508del-CFTR demonstrated that the delivery mechanism to degradation depends on K8 recruitment to the ERAD complexes (Fig. 7).

A small molecule, c407, increases the secretion of Z-A1AT and is an ERAD modulator

To test if K8-containing ERAD complexes were druggable, we measured the WT-A1AT/Z-A1AT secretion upon treating HeLa and primary human nasal epithelial (HNE) cells with the c407 compound, previously found to disrupt K8–F508del-CFTR interaction and to correct CFTR trafficking

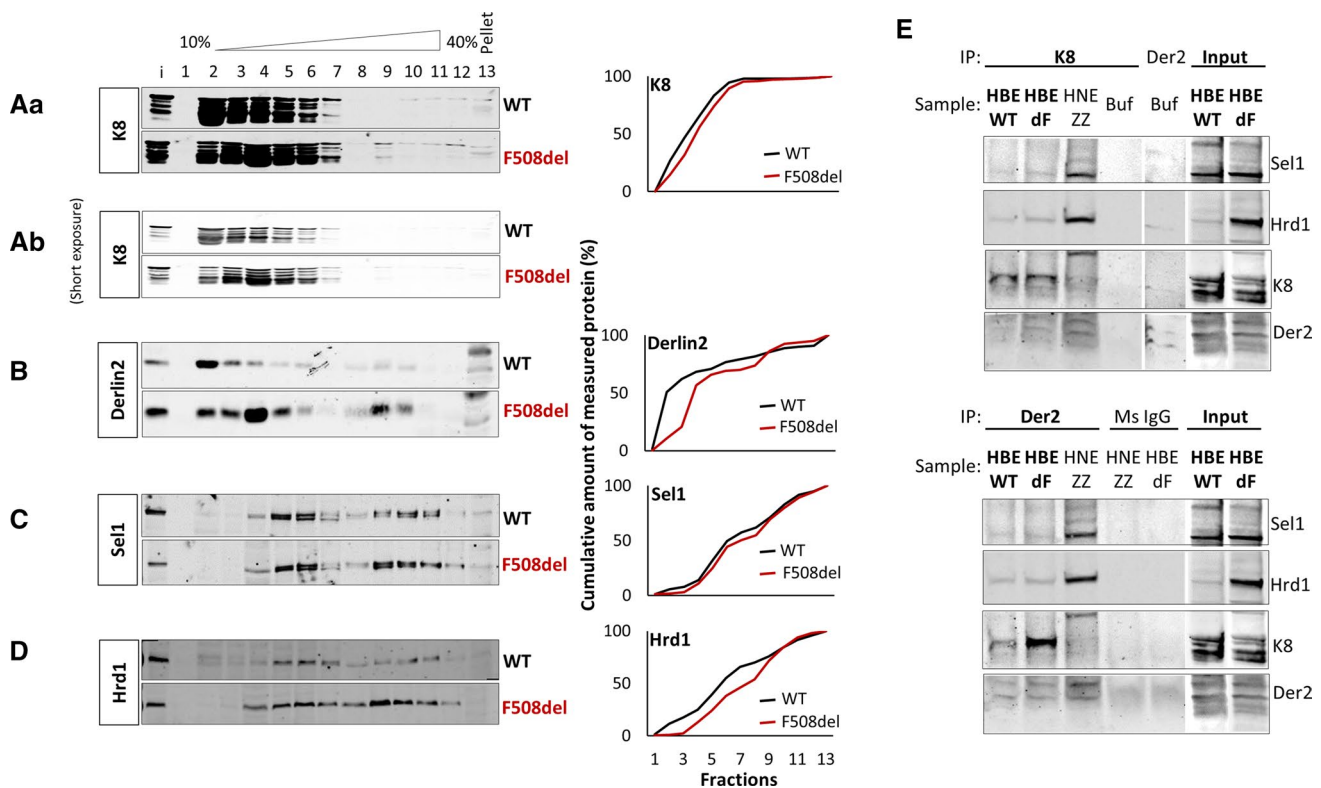


Fig. 5 K8 is recruited to the ERAD complexes upon overexpression of misfolded F508del-CFTR. 16HBE cells expressing WT-CFTR and F508del-CFTR, as indicated, were lysed in 1% w/v LMNG and sedimented over a 10–40% w/v sucrose gradient. Levels of K8 (**Aa** and **Ab**), Hrd1 (**D**), Sel1 (**C**), Derlin-2 (**B**), were detected by immunoblotting. Representative images are shown. Quantifications represent results shown in the corresponding images on the left and are expressed as cumulative amount of measured protein (%) to demonstrate the overall shift. Experiment was performed three times. **E**

Co-immunoprecipitation of ERAD complexes from microsomes of 16HBE cells expressing WT- or F508del-CFTR. Derlin2 or K8 were immunoprecipitated with anti-Derlin2 (top panel) or anti-K8 antibodies (bottom panel), respectively (see Methods section) and proteins of interest were detected using corresponding antibodies (Sel1, Hrd1, K8, Derlin2). Negative controls with unspecific mouse IgG (Ms IgG) and extracts, as well as with anti-Derlin2/K8 antibody and LMNG buffer were applied

to the plasma membrane [38]. Treatment of both cell types resulted in an increase of Z-A1AT secretion in the concentration range of 10–35 μ M (Fig. 6A, B), 20 μ M c407 being the most efficient. In both primary HNE and HeLa cells, c407 did not affect WT-A1AT secretion.

To test whether c407 targeted K8 directly, structure stabilization experiments were performed using HDex-MS (hydrogen–deuterium exchange mass spectrometry) on purified K8. The addition of c407 (Supp. Fig. 7A, B) induced the stabilization of multiple regions of K8, suggesting c407-K8 direct interactions. In solution, K8 was shown to exist as dimers in two distinct forms—a folded dimeric form stabilized by head-rod domain interactions and an unfolded dimeric form, as demonstrated by HDex-MS analysis [44]. The robust allosteric stabilization observed in the K8 head domain peptides 2–19 (Supp. Fig. 7A, first panel) and the rod domain peptides (Supp. Fig. 7A, B) suggest a likely shift in the equilibrium to the folded form of the K8 dimer. These results were supported by observations from

immunocytochemistry experiments showing partial recovery of K8 network after c407 treatment in HeLa cells expressing Z-A1AT and 16HBE cells expressing F508del-CFTR (Supp. Fig. 8A, B). Sucrose gradient fractionation of c407 treated HeLa cell lysates showed a less important shift of K8 and Derlin2 to heavy fractions compared to untreated cells (Fig. 6C), while Hrd1 and Sel1 were not affected. Moreover, Derlin2 co-distributed with K8 both in control conditions and after treatment with c407 according to immunocytochemistry (Supp. Fig. 8C, D). Altogether, these results suggest that targeting the K8–Derlin 2 complex with c407 enhances Z-A1AT secretion.

Discussion

In this study, we shed light on a new role of K8 as a scaffolding factor of ERAD protein complexes in epithelial cells (Fig. 7). We demonstrated that K8 negatively regulates

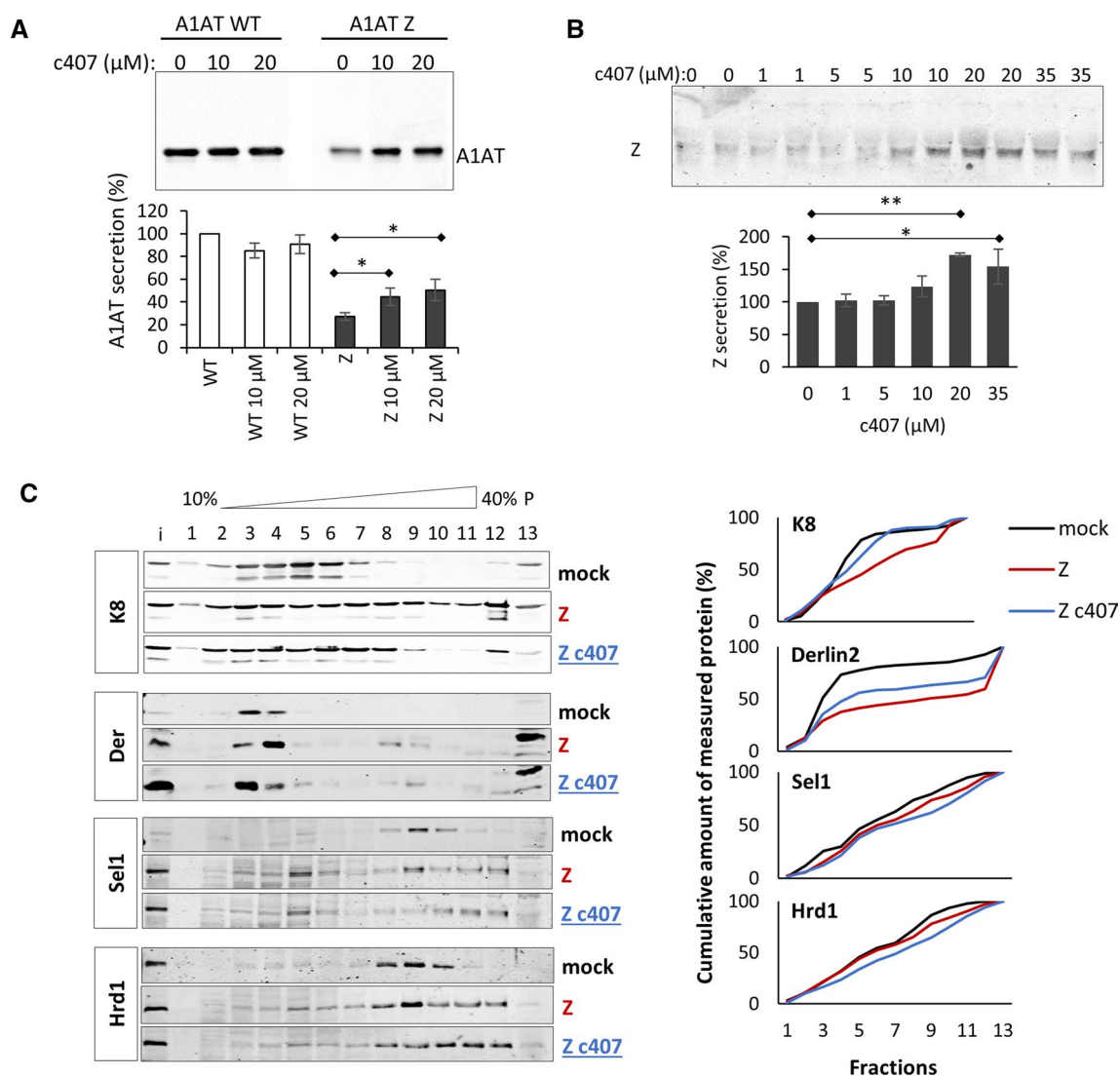


Fig. 6 Compound c407 increases secretion of Z-A1AT from HeLa and primary HNE cells through modulating K8-containing ERAD complexes. **A** Quantification of WT-A1AT and Z-A1AT secretion level from HeLa cells upon treatment with c407 (10 and 20) and vehicle (0). Cells were treated with c407 at concentrations of 10 and 20 μ M for 24 h. The representative WB analysis image shows A1AT secreted into the medium. **B** Quantification of Z-A1AT secretion level from primary HNE cells upon treatment with c407 (1, 5, 10, 20 and 35) and vehicle (0). Cells were treated with c407 at concentrations of 1, 5, 10, 20 and 35 μ M for 14 days as pre-treatment and for 24 h for

test of secretion. The representative WB analysis image shows A1AT secreted into the medium. **C** Sucrose gradient fractionation results upon c407 treatment. HeLa cells were transfected with Z-A1AT (Z) and treated with c407 at concentration of 20 μ M or vehicle for 48 h, as indicated. Levels of K8, Hrd1, Sel1, and Derlin-2 were detected by immunoblotting in all fractions. Representative images are shown. Quantifications represent results shown in the corresponding images on the left and are expressed as cumulative amount of measured protein (%) to demonstrate the overall shift. Experiment was performed three times

secretory trafficking of misfolded Z-A1AT, as it was the case for F508del-CFTR [7]. Consequently, decreased K8 expression compromised ERAD leading to enhanced apoptosis of heavy chain μ_s -expressing cells. Finally, in three cell models, HeLa, HBE and polarized primary HNE cells, we provided evidence of K8 implication in the ERAD processes by demonstrating K8 recruitment to complexes containing Derlin2, Hrd1 and Sel1 proteins and thus modulation of Hrd1-orchestrated processes (Fig. 7). Altogether, these data suggest that

K8 participates in retrotranslocation initiation and ubiquitination of Z-A1AT, F508del-CFTR, μ_s and to some extent WT-A1AT and WT-CFTR. This unveils new structural and regulatory features of K8 within ERAD.

Misfolded Z-A1AT and F508del-CFTR are in soluble complexes with multiple ER chaperones [27, 50]. They are substrates for the ERAD pathway [2, 14, 61] orchestrated by Hrd1-dependent ubiquitination at an early step [47, 63]. We showed agreement with previously published results [23]

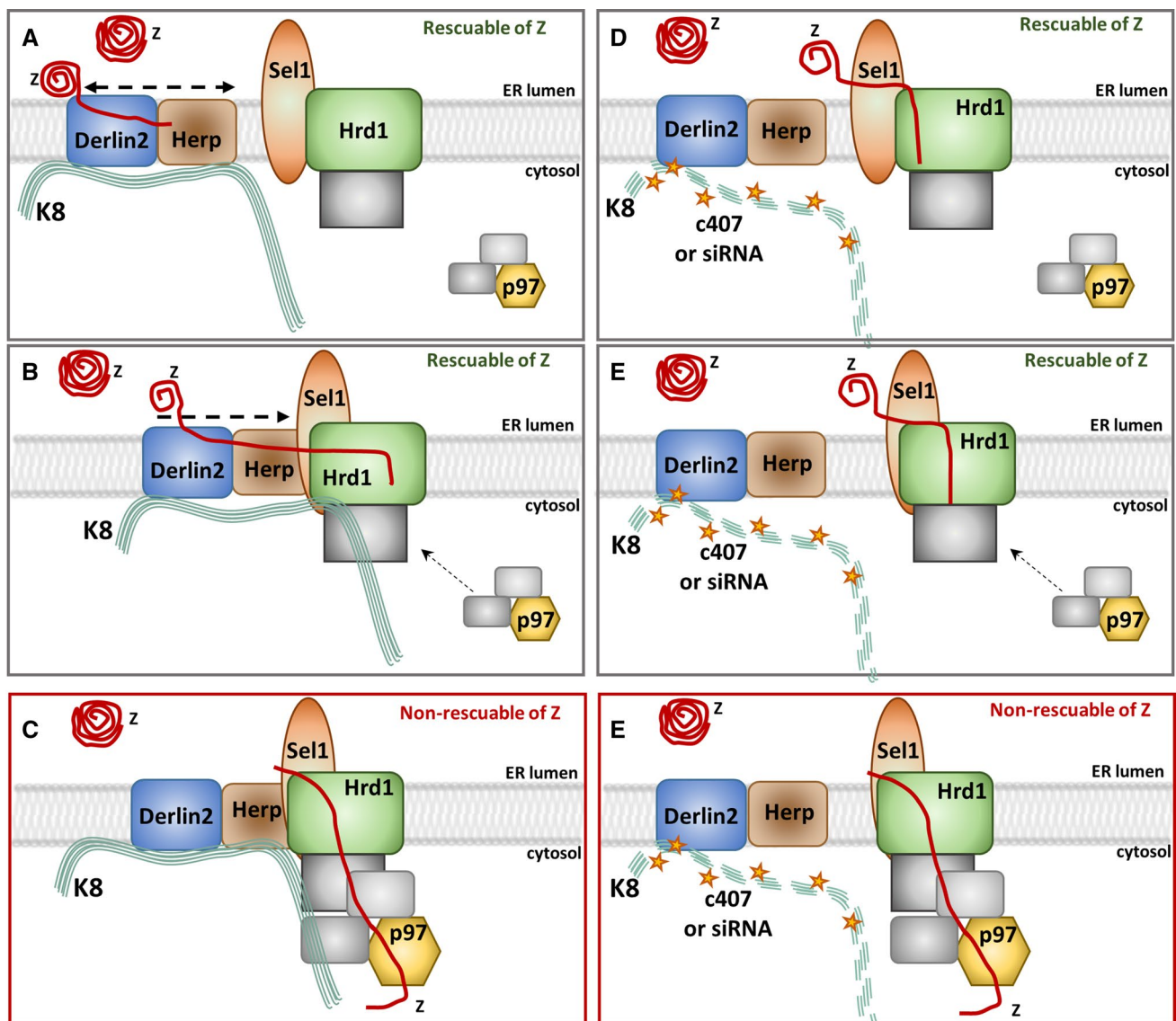


Fig. 7 Model of K8 recruitment to the ERAD complexes at the ER membrane—hypothesis (Adapted from Christianson and Ye). Normal K8 recruitment to the ERAD complexes: **A** K8 as a scaffolding platform in constant complex with Derlin2. Z-A1AT is recognized and recruited for retrotranslocation and ubiquitination. Stage rescuable for Z-A1AT secretion (upon Hrd1 or K8 down-regulation). Low density fractions complexes containing Derlin2 (module 2A in Supp. Fig. 1). **B** K8 facilitates complexing with Hrd1/Sel1. Retrotranslocation of ubiquitinated Z-A1AT is initiated. Stage rescuable for Z-A1AT secretion (upon Hrd1 or K8 down-regulation). Medium to high-density fractions complexes containing Derlin2, Sel1 and Hrd1 (modules 2A+2B in Supp. Fig. 1). **C** Z-A1AT is being dislocated from the ER lumen to the cytosol. Dislocation stage no rescuable for Z-A1AT secretion (upon p97 inhibition). Hypothetic higher-order complexes

containing Derlin2, Sel1, Hrd1 and p97. Decreased or no recruitment of K8 to the ERAD complexes upon c407 molecule treatment or siRNA against K8: **D** K8–Derlin2 complex maintained (low-density fractions) even with residual K8. However, K8-dependent scaffolding of higher-order complexes is affected. Recruitment of Z-A1AT for retrotranslocation and ubiquitination is reduced. ER-luminal Z-A1AT is secreted. **E** K8–Derlin2 is not recruited to form complexes with Hrd1/Sel1. The shRNAK8 decreases Sel1 and Hrd1 recruitment to high-order complexes. By contrast, c407 treatment of cells do not change Hrd1 and Sel1 recruitment to higher-order complexes. Retrotranslocation initiation and ubiquitination of Z-A1AT is reduced. ER-luminal Z-A1AT is secreted. **F** Z-A1AT dislocation to the cytosol is reduced. ER-luminal Z-A1AT is secreted

that Hrd1 knock-out led to the rescue of Z-A1AT secretion. K8 probably acts at this early step of ERAD, as it is recruited to the Hrd1–Derlin2 complexes. Furthermore, knocking out Hrd1, but not inhibiting p97, led to the rescue of the A1AT secretion. Altogether, these results suggested that reducing

K8 expression diminishes ERAD efficacy, increases Z-A1AT maturation and, consequently, enhances Z-A1AT secretion. We postulate that K8 is a novel actor regulating ERAD. Furthermore, retrotranslocation is a crucial checkpoint defining rescuable and non-rescuable forms of misfolded proteins.

This limit could be between Derlin2–Hrd1- and p97-governed steps of ERAD degradation when the retrotranslocated substrate is undergoing dislocation (Fig. 7 A, B vs C).

We propose that K8 serves as a scaffolding platform on which other ERAD proteins build up functional complexes (Fig. 7). Different phases of retrotranslocation and ubiquitination are highly dynamic and create multiple stable and transient complexes upon stimuli [15]. Therefore, it is not surprising that K8 can be recruited to many of them (Fig. 7) to facilitate transitions and remodeling of these complexes. The precise organization of the retrotranslocating complexes is still not known. However, the involvement of the Hrd1–Hrd3 (Sel1) complex [51], Derlin family members [30, 66], and the Hrd1–Der1 complex [64] has been shown. Importantly, our results suggest that (i) K8–Derlin2 complexing is relatively permanent (detected even in mock cells and in cells with reduced K8 expression) and (ii) the recruitment of other ERAD proteins (Hrd1 and Sel1) occurs upon expression of misfolded Z-A1AT.

It could be argued that K8, an abundant protein in epithelial cells, binds non-specifically to intracellular protein complexes. However, as shown by immunocytochemistry, the intracellular distribution of K8 differed between Z-A1AT vs WT-A1AT-expressing HeLa and patient-derived HBE cells. It has also been previously observed for patients' derived HBE cells expressing F508del-CFTR or WT-CFTR [7]. Moreover, non-specific K8 recruitment to ERAD complexes would be expressed as K8 sedimentation into all fractions in the shK8 cell and in mock-transfected cell lysates, which is not the case.

We postulate that keratins are essential regulators of processes occurring at the endoplasmic reticulum (ER) and Golgi. K18, which forms a heterodimer with K8, also plays a role in F508del-CFTR trafficking [11] by binding to the C-terminus of CFTR while K8 binds to the NBD1 domain [7, 13]. Similarly to K8, K18 may be involved at the ER level [57]. Importantly, silencing K18 leads to the rescue of F508del-CFTR function [11]. On another hand, K18 co-distributes with WT-/Z-A1AT, but the absence of increase of proximity to Z-A1AT in PLA assay (in contrast to K8), suggest that K18 may also be indirectly implicated in ERAD scaffolding. This also reinforces the idea that different rescue mechanisms implicating intermediary filaments exist within ERAD.

Our results are supported by other reports which also indicated that keratins are important proteins regulating processes at the ER and Golgi. K8 specifically binds Hsp70 involved in the ERAD pathway [29, 49] and K1, belonging to the same family of proteins as K8, forms complexes responsible for the retention of N-acetylglucosaminyltransferase within the Golgi structures [42].

A small-molecule c407, which disrupts the interaction between F508del-CFTR and K8 [38], and which long-term

administration is not toxic in mice [10] increased Z-A1AT secretion in Z-A1AT-expressing HeLa cells, and importantly, in a more physiological model, differentiated primary HNE cells expressing endogenous Z-A1AT, providing preclinical evidence of potential therapeutic. Because c407 modified K8 and Derlin2 recruitment to ERAD complexes, we propose that K8–Derlin2 complexes represent a potent target for pharmacotherapy. However, c407 treatment did not completely disrupt ERAD complexes because Sel1 and Hrd1 profiles did not change. Such an effect, if it occurred, would be toxic for cells and therefore inappropriate for therapy. Alternatively, the implication of K18 in ERAD scaffolding cannot be excluded. C407 also failed to increase WT-A1AT secretion, contrary to reduced K8 expression, indicative of incompletely overlapping mechanisms of action. Using HDex-MS analysis, we showed that c407 stabilizes multiple regions of K8, consistent with direct binding, which may lead to decreased interactions of K8 with other proteins and less efficient formation of protein complexes. Importantly, c407 allowed to restore K8 network which became similar to WT-A1AT expressing cells. HDex-MS experiments on Z-A1AT could not be performed due to its self-polymerisation.

Targeting the early steps of ERAD enables overcoming the difficulties of binding to highly mobile folding intermediates of Z-A1AT [33]. One of the early ERAD proteins, Hrd1, has been proposed as a direct therapeutic target for several diseases: rheumatoid arthritis [46, 65], type 2 diabetes [64], Alzheimer's and Parkinson's diseases [37]. Pharmacological or genetic inhibition of Hrd1 significantly reduced the severity of rheumatoid arthritis and glucose control in the diabetic model. By contrast, in Alzheimer's and Parkinson's diseases, Hrd1 overexpression leads to suppression of Pael-R- or Aβ1–40 and Aβ1–42-induced cell death [37]. Our therapeutic strategy, based on modulation of K8-regulated early ERAD complexes with chemical compounds opens new perspectives for A1ATD and other epithelial protein misfolded diseases (PMDs). The preliminary results obtained in mouse model of nephrotic syndrome due to the mutation in podocin, R138Q, support this hypothesis (Kuzmuk et al., abstract SA-OR-052, Kidney Week 2019). Combining molecules targeting the misfolded protein directly [33] with molecules affecting ERAD (e.g., c407) could lead to enhanced rescue.

In conclusion, we demonstrated that K8 is a scaffolding factor for early-stage ERAD complexes regulating the degradation of ERAD substrates and propose targeting ERAD complexes containing K8 as an attractive strategy for the pharmacotherapy of A1AD and possibly other epithelial PMDs.

Materials and methods

Cell culture

HeLa cells

HeLa cells transiently transfected with pcDNA3-WT-A1AT or Z-A1AT were cultured in Dulbecco's modified eagle medium (DMEM) and were supplemented with 10% v/v fetal calf serum (FCS), 2 mM L-glutamine, 100 µg/ml streptomycin and 100 units/ml penicillin in a humidified incubator at 37 °C 5% v/v CO₂. WT-A1AT/Z-A1AT cDNA was kindly provided by Prof. Eric Chevet (University of Bordeaux, France). Western blot (WB) analysis of WT-A1AT and Z-A1AT extracted from transiently transfected HeLa cells revealed that Z-A1AT-expressing cells produced less fully glycosylated A1AT than cells transfected with WT-A1AT (Supp. Fig. 9A, upper left panel) concomitant with reduced secretion, reaching only 25% of WT secretion level (Supp. Fig. 9A, bottom left panel and quantification).

We generated HeLa cells that express reduced amounts of K8 using the shRNA approach (shK8 HeLa cells). WB quantification showed that shK8 HeLa cells expressed ~17% of the normal K8 level (Supp. Fig. 9C, D); transient transfection with either WT-A1AT or Z-A1AT did not affect this level (Supp. Fig. 9C).

HeLa cell lines stably expressing the IgM heavy chain subunit μ_s under induction with Mifepristone (Mif, 0.5 nM), WT variant and Hrd1KO, were a kind gift from Dr Eelco van Anken (IRCCS Ospedale, San Raffaele, Italy). These cells were cultured in DMEM (Dulbecco's modified eagle medium) and were supplemented with 5% v/v FCS, 100 µg/ml streptomycin and 100 units/ml penicillin in a humidified incubator at 37 °C and 5% v/v CO₂.

HeLa cells are derived from simple epithelium cells, the same type of epithelium as respiratory epithelium and hepatocytes. Importantly, they endogenously express Keratin 8 and are easily transfected with plasmids coding for A1AT or with siRNA or transduced with shRNA. HeLa cells are a relevant tool to largely explore the mechanisms observed in physiological context using HBE cells.

16HBE WT and F508del cell lines

16HBE WT cells (full name 16HBE14o- Human bronchial epithelial cell line) are human bronchial epithelial cells isolated from bronchial explant of a patient with WT-CFTR, immortalized with SV40 and clone selected. Cells contain only two copies of *CFTR* gene under natural non-modified expression system.

16HBE F508del cell line (16HBEge CFTR F508del—genetically engineered) used in the study was obtained from

Cystic Fibrosis Foundation (CFF) [58]. This cell line was created from 16HBE14o- cells by CRISPR/Cas9 methodology to introduce the F508del mutation in the *CFTR* gene. Similarly to 16HBE14o- cells, 16HBEge CFTR F508del cells have two alleles of *CFTR* gene, but mutated.

16HBE cells are not transfected nor transduced with CFTR gene. CFTR protein expression is obtained from only two copies of a gene under natural promotor.

Primary HBE/HNE cells

The establishment of primary bronchial epithelial cell cultures from PiZZ AATD patients ($n=3$) and MM controls ($n=3$) matched according to sex, GOLD stage (0–III), and smoking status has been previously reported [59]. Cell cultures were re-established from liquid nitrogen stored stocks. Primary nasal epithelial cell cultures from PiZZ AATD patients ($n=2$) and MM control ($n=1$) were established from fresh nasal brushing [43]. In primary human bronchial epithelial (HBE) and human nasal epithelial (HNE) cells derived from Z-homozygous (PiZZ) or WT-homozygous individuals (Supp. Fig. 9C), the fraction of secreted A1AT was lower (<50%) in PiZZ cells than in WT cells. In contrast, intracellular levels of Z-A1AT was increased compared to WT-A1AT (compare Supp. Fig. 9C upper and lower panels).

Silencing K8 expression

K8 expression was silenced in HeLa cells using a stable shRNA (Thermo Scientific) transduced by lentiviral vectors. HeLa cells containing the shRNA construct and parental HeLa cells were transfected with pcDNA3-A1AT WT or A1AT Z. For the growth or secretion assay in Hrd1KO cells, K8 expression was silenced with siRNA (Dharmacon siRNA Reagents) transiently transfected into HeLa cells with DharmaFect Reagent (Dharmacon).

Protein sample preparation for immunoblotting

Cell lysis and cell extract preparation

Cells were first trypsinized and centrifuged at 300g for 10 min at 4 °C, washed on ice with phosphate-buffered saline (PBS) and recentrifuged at 300g for 10 min at 4 °C. The cell pellet was then resuspended in a lysis buffer composed of Tris-HCl pH 7.5, 20 mM, NaCl 50 mM, EDTA 1 mM, NP40 0.5% v/v and a protease inhibitor cocktail (cOmplete Tablets, Roche, 04 693 124 001) and incubated on ice for 30 min. Next, cell lysates were centrifuged at 1500 g for 15 min at 4 °C. Supernatants were transferred to a new set of tubes, and the protein concentration was measured with the DC

Protein Assay (BioRad, 500-0113, -0114, -0115) according to the manufacturer's protocols.

Preparation of the secreted protein

Cells were grown to 80–90% confluence and then washed three times with PBS to remove serum. Cultures were then kept in the DMEM media containing only penicillin/streptomycin for 24 h or shorter. Media with secreted proteins were collected, centrifuged at 300 g, divided into aliquots and frozen at -80°C . Each sample used for the WB analysis was defrosted once. Samples for mass spectrometry standard protein identification were sent to proteomic SFR Necker core facilities (<https://fr.sfr-necker.fr/proteomics>).

Western blot analysis

For protein detection by WB samples were mixed with a 5X Laemmli sample buffer and heated at 95°C for 5 min, resolved using a 10% w/v acrylamide SDS-PAGE gel and transferred to nitrocellulose membranes. The membranes were then incubated in a blocking buffer (3% w/v BSA (bovine serum albumin) and 3% w/v milk in PBS-0.1% v/v Tween-20) for 1 h. Proteins of interest were immunodetected with appropriate antibodies (ab) diluted in a 3% w/v BSA blocking buffer for 1 h. K8 was immuno-detected with mouse monoclonal ab (61,038, Progen) at a 1:500 dilution, A1AT was immuno-detected using the primary rabbit polyclonal anti-human A1AT ab (A0012, Dako, Agilent) at a 1:1000 dilution, Derlin2 was detected with mouse monoclonal ab (sc-398573, Santa Cruz Biot Inc.). Sell was detected with mouse monoclonal ab (sc-377350, Santa Cruz Biot Inc.), and Hrd1 was detected with rabbit anti-Synoviolin ab (A302-946A-M, Bethyl). Other abs used were: rabbit polyclonal anti-GAPDH (sc-25778, Santa Cruz Biot Inc.) at a 1:500 dilution, mouse anti- $\text{Na}^+\text{K}^+\text{ATPase}$ (ab7671, Abcam) at a 1:1000 dilution, mouse monoclonal anti-Hsp70 (sc-24, Santa Cruz Biot Inc.) at a 1:1000 dilution, rabbit anti-*Gaussia* luciferase (E8023, New England Biolabs) at a 1:2000 dilution, rat monoclonal anti-Grp78 (sc-13539, Santa Cruz Biot Inc.) at a 1:500 dilution and rabbit polyclonal anti-Calreticulin (SPA-600, Stressgen) at a 1:500 dilution. Finally, nitrocellulose membranes were incubated with appropriate secondary antibodies coupled to fluorochromes, as recommended by the manufacturer (Li-Cor, Bad Homburg, Germany). The detection of the WB results was performed with the Odyssey scanner (Li-Cor, Germany). Quantification of the WB was performed using ImageJ software.

Non-secreted (intracellular) WT-A1AT is detected in western blot in form of two bands, corresponding to non-mature—core-glycosylated (ER form) and mature—fully glycosylated protein (Golgi and post-Golgi form). Intracellular Z-A1AT present mainly one band corresponding to

non-mature/core-glycosylated protein (ER form) and a slight amount of mature/fully glycosylated protein (that escaped from degradation and aggregation in the ER). Secreted (fully glycosylated) WT-A1AT is detected as only one band. Similarly Z-A1AT if it escape the degradation pathway or aggregation in the ER, it passes through the Golgi to be glycosylated and then secreted.

Immunocytochemistry

HeLa and HBE cells were grown on microscopy slides up to low levels of confluence. The cells on the slides were washed twice with PBS and fixed with ice-cold acetone for 5 min. Next, the slides were washed twice with PBS, dried and stored at -20°C if necessary. The cells were then thawed, rehydrated with phosphate-buffered saline with 0.1% v/v Tween-20 (PBS-T) and incubated in blocking solution 3% w/v BSA in PBS-T for 1 h at room temperature (RT). Protein immunodetection was performed with primary abs diluted in blocking solution during overnight incubation at 4°C : rabbit polyclonal ab against alpha-1-antitrypsin (A0012, Dako, Agilent) at a 1:500 dilution, mouse monoclonal ab against K8 (61,038, Progen) at a 1:200 dilution, and goat polyclonal ab against Calnexin (Santa Cruz Biot Inc.) at a 1:500 dilution. The primary antibodies against different proteins were incubated simultaneously. Subsequently, the cells were washed four times for 5 min each in PBS-Tween20 0.1% v/v, and non-specific binding sites were blocked in 5% v/v goat serum (in PBS-Tween20) for 30 min. The cells were then incubated for 45 min at RT with goat secondary IgGs conjugated to Alexa 488 or 594 at a 1:1000 dilution in 5% v/v goat serum in PBS-T. After five washes for 5 min each, the Vectashield mounting medium containing DAPI (Vector Laboratories, H-1200) was used to mount the cells on microscope slides. Immunocytochemistry on the air–liquid interface cultures of the primary HBE cells was performed, as described previously [43].

Confocal microscopy

Confocal microscopy was performed as described previously [43]. Briefly, a Leica TCS SP5 AOBS confocal microscope (Heidelberg, Germany) was used. Multiple optical z-stack images were captured over the cell culture. The images were analyzed with ImageJ software (NIH, USA). The colocalisation level was assessed by the ImageJ plug-in JACoP and tools Image calculator and Measure stack. The PLA results were quantified with the Analyze Particles tool and expressed as an average number of fluorescent spots (nfs), minus the average number of negative controls.

Synthetic lethality assay (Growth assay)

HeLa cells overexpressing IgM heavy chain subunits μ_s under Tet-inducible promoter [1, 62] were kindly provided by Dr Eelco van Anken. In the absence of light chains, heavy chains cannot reconstitute IgM and cannot be secreted. The μ_s is retained in the ER, and its accumulation activates the unfolded protein response. Once the ERAD pathway is deactivated, heavy chains overload the ER leading to synthetic lethality through apoptosis, defining which factors are crucial to act in conjunction with Hrd1 and Sel1L in the disposal of μ_s [62]. The experiments were performed according to a previously published protocol [1]. The HeLa cells overexpressing IgM heavy chain subunit μ_s upon induction with 0.5 nM Mifepristone (Mif) were first transfected with siRNA directed against K8 and scrambled sequence (Dharmacon siRNA Reagents). Non-transfected cells and cells 24 h after transfection were trypsinized, counted with a Malassez chamber, and seeded upon 1:5 serial dilutions (5000, 1000, and 200 cells per well) in 24-well plates. Mifepristone (0.5 nM) was added after cells were attached to the growth surface. To assess growth differences between tested conditions, cells were grown for 7 days. Culture media and pharmacological agents were refreshed every 2–3 days. Cells were then fixed with methanol–acetone (1:1) for 10 min, stained with 0.5% crystal violet in 20% methanol for 10 min, and washed with distilled water afterwards. Dried plates were imaged with the ChemiDoc TM XRS+ (Bio-Rad). The intensity of crystal violet staining was quantified with ImageJ software (NIH). An average intensity of empty wells on the same plate served for background subtraction. Quantification of growth was presented for wells with a seeding of 1000 cells.

ERAD complexes fractionation

The experiments were performed as described in [62]. HeLa cells were grown on T75 flasks up to 75% of confluence and transfected with plasmids coding for WT-A1AT or Z-A1AT using the Lipofectamine 3000 protocol (Thermo Fisher Scientific). Additionally, heavy chains μ_s were induced with Mifepristone 0.5 nM 24 h before harvesting the cells. Cell lysis was performed 48 h post-transfection with a lysis buffer [50 mM Tris–HCl pH 7.4, 150 mM NaCl, 5 mM EDTA, 1% lauryl maltose neopentyl glycol (LMNG)] containing a mix of proteases inhibitors (cOmplete Tablets, Roche, 04 693 124 001). After centrifugation at 5000g for 10 min, cell lysates were loaded on the top of 10–40% linear sucrose gradients and centrifuged at 39,000 rpm/17 h/4 °C in a SW41Ti rotor. Sucrose gradients were prepared with a Hoefer gradient maker. The 13 fractions were collected from low density at the top of the gradient to high density at the bottom. Proteins were precipitated with trichloroacetic acid and

washed with ice-cold acetone. Protein pellets were resuspended in a Laemmli buffer containing dithiothreitol (DTT, 10 mM), heated at 50 °C before separation by SDS-PAGE. After protein transfer to nitrocellulose membrane, proteins were detected with appropriate antibodies: K8-mouse monoclonal ab (61,038, Progen), Sel1 (sc-377350, Santa Cruz Biot Inc.), Hrd1/Synoviolin (A302-946A-M, Bethyl), and Derlin2 (sc-398573, Santa Cruz Biot Inc.). The intensity of each protein band was measured using ImageJ (NIH Bethesda) and expressed as % of a sum of all fractions.

Preparation of cell microsomes

The cells grown in flasks were washed with PBS, trypsinized and centrifuged at 300g for 5 min at 4 °C. The cell pellet was washed twice in PBS, recentrifuged at 300 g for 5 min at 4 °C and resuspended in 800 μ l of the isotonic extraction buffer (10 mM HEPES, pH 7.8, 250 mM sucrose, 25 mM potassium chloride and 1 mM EDTA) in the presence of a protease inhibitor cocktail (Roche). Cell lysis was performed using mechanical homogenisation with constant incubation of the samples on ice. Up to 70% of the sample showed disrupted cells when observed under microscope. The homogenized cells were then transferred to prechilled 1.5 ml tubes and centrifuged at 6000g for 10 min at 4 °C; the collected supernatant was recentrifuged in a fresh tube at 9000 g for 15 min at 4 °C. A new supernatant was collected in a prechilled 1.5 ml ultracentrifuge tube and centrifuged at 100,000g for 1 h at 4 °C in a TLA-55 rotor (Beckman Coulter). The resulting pellet was resuspended in the same isotonic buffer containing antiproteases and was frozen at – 80 °C together with the 100,000g supernatant, which represented the cytosolic fraction.

Co-immunoprecipitation

HeLa cells were grown on 4 T75 culture flasks up to 75–85% confluence, transfected with WT- or Z-A1AT, and collected by trypsinisation 48 h after transfection. 16HBE cells were grown on 4 T75 flasks and maintained in 100% confluence for 3–4 days, and trypsinized. Polarized primary HNE cells were grown and differentiated on microporous filters for 3 weeks, washed twice with PBS and collected directly before cell lysis by scraping in isotonic lysis buffer. The cell pellets (HeLa and 16HBE cells) were washed twice with PBS and then resuspended in isotonic lysis buffer (see protocol Preparation of microsomes) with addition of protease inhibitor cocktail (Roche) and homogenized on ice with mechanic homogenizer. Cell lysates were then sequentially centrifuged as described in protocol Preparation of microsomes to obtain microsomes pellet. The resulting pellet was resuspended in lysis buffer containing LMNG detergent (see protocol ERAD complexes fractionation) containing a mix

of proteases inhibitors. Next, Dynabeads Protein G beads were washed twice with PBS-Tween20 0.01% v/v and incubated with an antibody solution (1 µg/20 µl of beads) containing anti-Derlin2 antibody (sc-398573, Santa Cruz Biot Inc.) or anti-K8 (ref 61,038, Progen, Germany) for 1 h at RT with constant rotation. A negative control with mouse IgG (ref 12–371, Merck-Millipore) was prepared using the same protocol. The beads were washed with PBS-Tween20 0.01% v/v, and a DSS crosslinker was added at a final concentration of 100 µM for 15 min, which then was quenched by addition of Tris-HCl pH 7.5. The beads with the cross-linked antibody were mixed with cell lysates and incubated for 2 h at 4 °C at a constant rotation. After incubation, cell lysates were removed, and the beads were washed three times with LMNG lysis buffer (containing 1.5% of LMNG); the immunoprecipitated proteins were eluted with a Laemmli sample buffer at 37 °C for 15 min.

Proteinase K assay on the microsomal fraction

The Proteinase K assay, as adapted from Besingi and Clark [3], was designed to detect the presence or absence of a K8 protein in the interior of the ER/microsomal compartment or at the cytosolic periphery of the ER membrane. HeLa cells transfected with cDNA A1AT were grown in a T150 culture flask, trypsinized, washed with PBS and pelleted at 300g for 5 min at 4 °C. The microsomal fraction was purified, as described in the section ‘Cell microsomes preparation’. The microsomes were resuspended in the isotonic buffer. Each of the samples containing the microsomes was divided into two volumes. The first half of the microsomes was diluted in the same isotonic buffer, and the second was diluted in the isotonic buffer containing 1% v/v Triton X-100 (final Triton X-100 concentration 0.5% v/v) and incubated for 15 min to solubilize membranes and release intramicrosomal proteins. Next, the two samples (with and without Triton X-100) were divided to retain a nondigested aliquot, Proteinase K was added to the second aliquot to a working concentration of 125 µg/ml. It is assumed that Proteinase K digests all proteins in Triton X-100-treated samples and only externally/transmembrane-located proteins in non-treated samples. All samples—(i) microsomes in isotonic buffer; (ii) microsomes in isotonic buff. + Proteinase K; (iii) microsomes + Triton X-100; (iv) microsomes + Triton X-100 + Proteinase K—were incubated at 37 °C for 20 min. All samples were resolved on 10% SDS-PAGE gels and immunoblotted to detect A1AT (Dako, Agilent), K8 (Progen, Germany), Calreticulin (Stressgen) and Na⁺K⁺ATPase (Abcam).

Proximity ligation assay

Cells were grown on microscopy cover slips up to 50–60% confluence. The cells were washed twice with PBS and fixed with ice-cold acetone for 5 min. Afterwards, the slides were washed twice with PBS and dried before being stored at -20 °C. The PLA experiments were performed according to the manufacturer’s instructions (Olink). First, the cells were humidified with PBS-Tween 20 0.1% v/v and incubated in a blocking solution provided with the kit for 30 min at 37 °C. Next, the two primary anti-K8 mouse monoclonal (Progen) and anti-A1AT rabbit polyclonal (Dako) antibodies were diluted in dilution buffer (Olink) for 1 h at 37 °C. After three washes with TBS-Tween 20 0.1% v/v, the cells were incubated with the PLA probes (secondary abs provided by Olink) specific to primary mouse and rabbit IgGs and were coupled with the oligonucleotides for 1 h at 37 °C. The cells were then washed three times with TBS-T and incubated with a ligation mixture composed of the ligase and oligonucleotide-connectors (sequences homologous to the oligonucleotides conjugated with PLA probes). Connectors can hybridize with PLA probes only when the distance between the proteins is < 40 nm and then will form an enzymatically ligated circle. In the next step, after washing with TBS-T, the polymerization mixture with polymerase and nucleotides coupled with fluorochromes were added for amplification of the circular oligonucleotides as a template, using the PLA probe sequences as primers. Cells were mounted on microscopy slides with a Vectashield mounting medium containing DAPI. The negative controls were prepared using an identical procedure but by applying only one of the primary antibodies. Included positive control presents interaction between A1AT and Calnexin.

Cell culture treatments

HeLa cells treatments with the VCP/p97 inhibitor Eeyarstatine I (10 µM, Sigma Aldrich) in DMSO were done for 8 h, and NMS-873 (1 µM, Selleckchem) in DMSO for 20 h, at 37 °C in the CO₂ incubator. HeLa cells were treated with 5 µg/ml Brefeldin A for 7 h at 37 °C in the CO₂ incubator. Mifepristone was used at concentration of 0.5 nM for 6 days in the growth assay or for 48 h for secretion assay. Corrector molecule c407 was tested at final concentrations of 1, 5, 10, 20, and 35 µM. Wortmannin (1 µM) and MK-2206 (5 µM) for 20-h treatment of HeLa cells.

HDX-MS workflow and analysis

The HDX-MS experiments were performed as described previously (38), but with some minor modifications. Briefly, the undeuterated and deuterated WT-A1AT samples in their unbound and bound states were digested online

using a 2.1 mm × 30 mm immobilized pepsin resin column (Porozyme, ABI, Foster City, CA) with 0.07% v/v formic acid in water as the mobile phase (200 µl/min flow rate). The peptides were passed directly to the 2.1 mm × 5 mm C18 trapping column (ACQUITY BEH C18 VanGuard precolumn, 1.7 µm resin; Waters, Milford, MA). The trapped peptides were eluted onto a reversed phase column (Acquity UPLC BEH C18 column, 1.0 × 100 mm, 1.7 µm resin, Waters, Milford, MA) using an 8–40% gradient of acetonitrile in 0.1% v/v formic acid at 90 µl/min, which was controlled by the nanoACQUITY Binary Solvent Manager. The total time of a single run was 13.5 min. All fluidics, valves and columns, except for the pepsin digestion column, were maintained at 0.5 °C using the HDX Manager (Waters, Milford, MA). The C18 column outlet was coupled directly with the ion source of the SYNAPT G2 HDMS mass spectrometer (Waters, Milford, MA) while working in the ion mobility mode. Lock mass was activated and carried out using Leucine-enkephalin (Sigma). For protein identification, the mass spectra were acquired in the MSE mode over a m/z range of 50–2000. The spectrometer parameters were as follows: ESI-positive mode, capillary voltage 3 kV, sampling cone voltage 35 V, extraction cone voltage 3 V, source temperature 80 °C, desolvation temperature 175 °C and desolvation gas flow 800 L/h. The spectrometer was calibrated using standard calibrating solutions. Peptides were identified using the ProteinLynx Global Server software (PLGS, Waters, Milford, MA). The list of identified peptides containing peptide m/z, charge, retention time and ion mobility/drift time was passed to the DynamX 3.0 data analysis program (Waters, Milford, MA). The average masses of the peptides in the exchange experiment (Mex) at different incubation times (0 s (M_{ex}^0)—10 s, 1 min, 5 min, 30 min, 150 min and 1440 min (M_{ex}^{MAX}))—obtained from the automated analysis were then verified by visual inspection. Ambiguous or overlapping isotopic envelopes were discarded from further analysis. The fraction of deuterium exchanged by a given peptide was calculated according to Eq. 1 (Eq. 1), as follows:

$$\text{Fraction Exchanged} = \frac{M_{ex} - M_{ex}^0}{M_{ex}^{MAX} - M_{ex}^0}. \quad (1)$$

Error bars for the difference in deuteration were calculated as the standard deviations of three independent experiments. A student's *t* test for two independent samples with unequal variances and unequal sample sizes (also known as Welch's *t* test) was carried out to evaluate the differences in fractions exchanged between the same peptides in two different states. The final figures were plotted either using OriginPro 8.0 (OriginLab) software or R-project for Statistical Computing.

Statistics

The experiments were repeated at least three times. The results are expressed as mean ± SD and analyzed using Mann–Whitney test or as described for specific experiments.

Supplementary Information The online version contains supplementary material available at <https://doi.org/10.1007/s00018-022-04528-3>.

Acknowledgements The authors thank Dr. Eric Chevet for A1AT/Z-A1AT plasmids, Annemarie van Schadewijk for help in culturing the HBE cells, and Anush Bakhunts for µ₈ expressing HeLa cells. We thank Dr Grazyna Faure, Dr. Stefano Fumagali and Dr Olivier Namy for helpful discussions and advices. We thank Muriel Girard, Dominique Debray, Francois Vermeulen, Linda Boulanger and Marianne Schulte for providing the A1AT/Z-A1AT primary cells and Prof. Hideki Nishitoh for HEK Derlin1/2 KO cells. We thank Dr Chiara Guerrero and Dr Joanna Lipecka from Proteomic SFR Necker core facility for protein identifications. We are very grateful to Isabelle Hatin for technical assistance, and the cell imaging platform for assistance with microscopy experiments. The authors are very grateful to Mucoviscidose ABCF2 for support.

Author contributions IMP participated in the experimental strategy preparation, conceived the protocols, performed experiments, analyzed and interpreted results and wrote the manuscript; BC performed biochemistry experiments; AP performed mass spectrometry experiments and analysis; NB and KFT performed some biochemistry experiments; SB established the shRNAK8 cell line; DT performed cell biology experiments; AG participated in primary cell culture and biochemistry experiments; JS provided the A1AT/Z-A1AT primary cells; GLL participated in the experimental strategy preparation; PSH, MD and DAL participated in the writing of the manuscript; JAI participated in preparing the experimental strategy and edited the manuscript; AD-M participated in designing the experimental strategy and editing of the manuscript; EA participated in preparing the experimental strategy; AH performed cell biology experiments and wrote the manuscript; IS-G participated in preparing the experimental strategy and writing of the manuscript; AE conceived of and coordinated the project and wrote the manuscript. All authors reviewed the manuscript and approved its submission.

Funding This work was supported by Agence Nationale de la Recherche (ANR-13-BSV1-0019-01, and ANR-18-CE14-0004) and Chancellerie des universites de Paris (legs Poix, 15LEG005_9UMS1151).

Availability of data and materials The datasets generated during and/or analyzed during the current study are available from the corresponding author on reasonable request.

Declarations

Conflict of interest The authors have no relevant financial or non-financial interests to disclose.

Ethics approval and consent to participate This study was performed in line with the principles of the Declaration of Helsinki. Approval was granted by the Ethics Committee of Ile-de-France 2 (CPP IDF2: 2010–05-03–3). Written informed consent was obtained from all individual participants included in the study or parents of children under 16.

Consent to publish Not applicable.

Author comments This data has been published on a pre-print server bioRxiv (<https://www.biorxiv.org/content/10.1101/2022.02.01.478623v1>).

References

- Bakunts A, Orsi A, Vitale M et al (2017) Ratiometric sensing of BiP-client versus BiP levels by the unfolded protein response determines its signaling amplitude. *Elife* 6:e27518. <https://doi.org/10.7554/eLife.27518>
- Baldrige RD, Rapoport TA (2016) Autoubiquitination of the Hrd1 ligase triggers protein retrotranslocation in ERAD. *Cell* 166:394–407. <https://doi.org/10.1016/j.cell.2016.05.048>
- Besingi RN, Clark PL (2015) Extracellular protease digestion to evaluate membrane protein cell surface localization. *Nat Protoc* 10:2074–2080. <https://doi.org/10.1038/nprot.2015.131>
- Carlson EJ, Pironzo D, Skach WR (2006) p97 functions as an auxiliary factor to facilitate TM domain extraction during CFTR ER-associated degradation. *EMBO J* 25:4557–4566. <https://doi.org/10.1038/sj.emboj.7601307>
- Chakraborty P, Teckman J (2014) Alpha-1-antitrypsin deficiency liver disease: science and therapeutic potential 50 years later. *J Gastroenterol Pancreatol Liver Disord* 1(3):1–9. <https://doi.org/10.15226/2374-815X/1/3/00113>
- Christianson JC, Ye Y (2014) Cleaning up in the endoplasmic reticulum: ubiquitin in charge. *Nat Struct Mol Biol* 21:325–335. <https://doi.org/10.1038/nsmb.2793>
- Colas J, Faure G, Saussereau E et al (2012) Disruption of cytokeratin-8 interaction with F508del-CFTR corrects its functional defect. *Hum Mol Genet* 21:623–634. <https://doi.org/10.1093/hmg/ddr496>
- Coulombe PA, Omary MB (2002) “Hard” and “soft” principles defining the structure, function and regulation of keratin intermediate filaments. *Curr Opin Cell Biol* 14:110–122. [https://doi.org/10.1016/s0955-0674\(01\)00301-5](https://doi.org/10.1016/s0955-0674(01)00301-5)
- Coulombe PA, Wong P (2004) Cytoplasmic intermediate filaments revealed as dynamic and multipurpose scaffolds. *Nat Cell Biol* 6:699–706. <https://doi.org/10.1038/ncb0804-699>
- da Cunha MF, Pranke I, Sassi A et al (2022) Systemic bisphosphonic acid derivative restores chloride transport in Cystic Fibrosis mice. *Sci Rep* 12(1):6132. <https://doi.org/10.1038/s41598-022-09678-9>
- Davezac N, Tondelier D, Lipecka J et al (2004) Global proteomic approach unmasks involvement of keratins 8 and 18 in the delivery of cystic fibrosis transmembrane conductance regulator (CFTR)/deltaF508-CFTR to the plasma membrane. *Proteomics* 4:3833–3844. <https://doi.org/10.1002/pmic.200400850>
- Dong X-M, Liu E-D, Meng Y-X et al (2016) Keratin 8 limits TLR-triggered inflammatory responses through inhibiting TRAF6 polyubiquitination. *Sci Rep* 6:32710. <https://doi.org/10.1038/srep32710>
- Duan Y, Sun Y, Zhang F et al (2012) Keratin K18 increases cystic fibrosis transmembrane conductance regulator (CFTR) surface expression by binding to its C-terminal hydrophobic patch. *J Biol Chem* 287(48):40547–40559. <https://doi.org/10.1074/jbc.M112.403584>
- El Khouri E, Le Pavec G, Toledano MB, Delaunay-Moisan A (2013) RNF185 is a novel E3 ligase of endoplasmic reticulum-associated degradation (ERAD) that targets cystic fibrosis transmembrane conductance regulator (CFTR). *J Biol Chem* 288:31177–31191. <https://doi.org/10.1074/jbc.M113.470500>
- Eura Y, Miyata T, Kokame K (2020) Derlin-3 is required for changes in ERAD complex formation under ER stress. *Int J Mol Sci* 21:6146. <https://doi.org/10.3390/ijms21176146>
- Fregno I, Fasana E, Bergmann TJ, et al (2018) ER-to-lysosome-associated degradation of proteasome-resistant ATZ polymers occurs via receptor-mediated vesicular transport. *EMBO J*. <https://doi.org/10.15252/embj.201899259>
- Garza RM, Sato BK, Hampton RY (2009) In vitro analysis of Hrd1p-mediated retrotranslocation of its multispanning membrane substrate 3-Hydroxy-3-methylglutaryl (HMG)-CoA reductase. *J Biol Chem* 284:14710–14722. <https://doi.org/10.1074/jbc.M809607200>
- Ghouse R, Chu A, Wang Y, Perlmutter DH (2014) Mysteries of α 1-antitrypsin deficiency: emerging therapeutic strategies for a challenging disease. *Dis Model Mech* 7:411–419. <https://doi.org/10.1242/dmm.014092>
- Glenn KA, Wen H, Dankle G (2012) Lectin-like ubiquitin ligases degrade alpha-1 antitrypsin-Z. *FASEB J* 26:1B112
- Graham KS, Le A, Sifers RN (1990) Accumulation of the insoluble PiZ variant of human alpha 1-antitrypsin within the hepatic endoplasmic reticulum does not elevate the steady-state level of grp78/BiP. *J Biol Chem* 265:20463–20468
- Herrmann H, Aepli U (2004) Intermediate filaments: molecular structure, assembly mechanism, and integration into functionally distinct intracellular Scaffolds. *Annu Rev Biochem* 73:749–789. <https://doi.org/10.1146/annurev.biochem.73.011303.073823>
- Jensen TJ, Loo MA, Pind S et al (1995) Multiple proteolytic systems, including the proteasome, contribute to CFTR processing. *Cell* 83:129–135. [https://doi.org/10.1016/0092-8674\(95\)90241-4](https://doi.org/10.1016/0092-8674(95)90241-4)
- Joly P, Vignaud H, Martino JD et al (2017) ERAD defects and the HFE-H63D variant are associated with increased risk of liver damages in alpha 1-antitrypsin deficiency. *PLoS ONE* 12:e0179369. <https://doi.org/10.1371/journal.pone.0179369>
- Kerem B, Rommens JM, Buchanan JA et al (1989) Identification of the cystic fibrosis gene: genetic analysis. *Science* 245(4922):1073–1080. <https://doi.org/10.1126/science.2570460>
- Khodayari N, Marek G, Lu Y et al (2017) Erdj3 has an essential role for Z variant alpha-1-antitrypsin degradation. *J Cell Biochem*. <https://doi.org/10.1002/jcb.26069>
- Khodayari N, Wang RL, Marek G et al (2017) SVIP regulates Z variant alpha-1 antitrypsin retro-translocation by inhibiting ubiquitin ligase gp78. *PLoS ONE* 12:e0172983. <https://doi.org/10.1371/journal.pone.0172983>
- Kim S, Skach W (2012) Mechanisms of CFTR folding at the endoplasmic reticulum. *Front Pharmacol* 3:201. <https://doi.org/10.3389/fphar.2012.00201>
- Kroeger H, Miranda E, MacLeod I et al (2009) Endoplasmic reticulum-associated degradation (ERAD) and autophagy cooperate to degrade polyomeric mutant serpins. *J Biol Chem* 284:22793–22802. <https://doi.org/10.1074/jbc.M109.027102>
- Liao J, Lowther LA, Ghori N, Omary MB (1995) The 70-kDa heat shock proteins associate with glandular intermediate filaments in an ATP-dependent manner. *J Biol Chem* 270:915–922. <https://doi.org/10.1074/jbc.270.2.915>
- Lilley BN, Ploegh HL (2004) A membrane protein required for dislocation of misfolded proteins from the ER. *Nature* 429(6994):834–840. <https://doi.org/10.1038/nature02592>. (PMID: 15215855)
- Lim Y, Kim S, Yoon HN, Ku NO (2021) Keratin 8/18 regulate the Akt signaling pathway. *Int J Mol Sci* 22(17):9227. <https://doi.org/10.3390/ijms22179227>
- Lomas DA, Evans DL, Finch JT, Carrell RW (1992) The mechanism of Z alpha 1-antitrypsin accumulation in the liver. *Nature* 357:605–607. <https://doi.org/10.1038/357605a0>
- Lomas DA, Irving JA, Arico-Muendel C et al (2021) Development of a small molecule that corrects misfolding and increases


- secretion of Z $\alpha 1$ -antitrypsin. *EMBO Mol Med* 13:e13167. <https://doi.org/10.15252/emmm.202013167>
34. Mashukova A, Forteza R, Salas PJ (2016) Functional analysis of keratin-associated proteins in intestinal epithelia: heat-shock protein chaperoning and kinase rescue. *Methods Enzymol* 569:139–154. <https://doi.org/10.1016/bs.mie.2015.08.019>
 35. Mehtash AB, Hochstrasser M (2019) Ubiquitin-dependent protein degradation at the endoplasmic reticulum and nuclear envelope. *Semin Cell Dev Biol* 93:111–124. <https://doi.org/10.1016/j.semcdb.2018.09.013>
 36. Nakatsukasa K, Huyer G, Michaelis S, Brodsky JL (2008) Dissecting the ER-associated degradation of a misfolded polytopic membrane protein. *Cell* 132:101–112. <https://doi.org/10.1016/j.cell.2007.11.023>
 37. Nomura J, Hosoi T, Kaneko M et al (2016) Neuroprotection by endoplasmic reticulum stress-induced HRD1 and chaperones: possible therapeutic targets for Alzheimer's and Parkinson's disease. *Med Sci* 4:14. <https://doi.org/10.3390/medsci4030014>
 38. Odolczyk N, Fritsch J, Norez C et al (2013) Discovery of novel potent $\Delta F508$ -CFTR correctors that target the nucleotide binding domain. *EMBO Mol Med* 5:1484–1501. <https://doi.org/10.1002/emmm.201302699>
 39. Okiyonedo T, Lukacs GL (2012) Fixing cystic fibrosis by correcting CFTR domain assembly. *J Cell Biol* 199:199–204. <https://doi.org/10.1083/jcb.201208083>
 40. Okiyonedo T, Veit G, Dekkers JF et al (2013) Mechanism-based corrector combination restores $\Delta F508$ -CFTR folding and function. *Nat Chem Biol* 9:444–454. <https://doi.org/10.1038/nchembio.1253>
 41. Perlmuter DH (2006) The role of autophagy in alpha-1-antitrypsin deficiency: a specific cellular response in genetic diseases associated with aggregation-prone proteins. *Autophagy* 2:258–263
 42. Petrosyan A, Ali MF, Cheng P-W (2015) Keratin 1 plays a critical role in golgi localization of core 2 N-Acetylglucosaminyltransferase M via interaction with its cytoplasmic tail. *J Biol Chem* 290:6256–6269. <https://doi.org/10.1074/jbc.M114.618702>
 43. Pranke IM, Hatton A, Simonin J et al (2017) Correction of CFTR function in nasal epithelial cells from cystic fibrosis patients predicts improvement of respiratory function by CFTR modulators. *Sci Rep* 7:7375. <https://doi.org/10.1038/s41598-017-07504-1>
 44. Premchandrar A, Kupniewska A, Tarnowski K et al (2015) Analysis of distinct molecular assembly complexes of keratin K8 and K18 by hydrogen-deuterium exchange. *J Struct Biol* 192:426–440. <https://doi.org/10.1016/j.jsb.2015.10.001>
 45. Rabinovich E, Kerem A, Fröhlich K-U, et al (2002) AAA-ATPase p97/Cdc48p, a cytosolic chaperone required for endoplasmic reticulum-associated protein degradation. *Mol Cell Biol* 22:626–634. <https://doi.org/10.1128/MCB.22.2.626-634.2002>
 46. Rahmati M, Moosavi MA, McDermott MF (2018) ER stress: a therapeutic target in rheumatoid arthritis? *Trends Pharmacol Sci* 39:610–623. <https://doi.org/10.1016/j.tips.2018.03.010>
 47. Ramachandran S, Osterhaus SR, Parekh KR, et al (2016) SYVN1, NEDD8, and FBXO2 proteins regulate $\Delta F508$ cystic fibrosis transmembrane conductance regulator (CFTR) ubiquitin-mediated proteasomal degradation. *J Biol Chem* 291:25489–25504. <https://doi.org/10.1074/jbc.M116.754283>
 48. Ruggiano A, Foresti O, Carvalho P (2014) ER-associated degradation: protein quality control and beyond. *J Cell Biol* 204:869–879. <https://doi.org/10.1083/jcb.201312042>
 49. Salas PJ, Forteza R, Mashukova A (2016) Multiple roles for keratin intermediate filaments in the regulation of epithelial barrier function and apico-basal polarity. *Tissue Barriers* 4:e1178368. <https://doi.org/10.1080/21688370.2016.1178368>
 50. Schmidt BZ, Perlmuter DH (2005) Grp78, Grp94, and Grp170 interact with alpha1-antitrypsin mutants that are retained in the endoplasmic reticulum. *Am J Physiol Gastrointest Liver Physiol* 289:G444–455. <https://doi.org/10.1152/ajpgi.00237.2004>
 51. Schoebel S, Mi W, Stein A, Ovchinnikov S, Pavlovicz R, DiMaio F, Baker D, Chambers MG, Su H, Li D, Rapoport TA, Liao M (2017) Cryo-EM structure of the protein-conducting ERAD channel Hrd1 in complex with Hrd3. *Nature* 548(7667):352–355. <https://doi.org/10.1038/nature23314>. (Epub 2017 Jul 6. PMID: 28682307; PMCID: PMC5736104)
 52. Shen Y, Ballar P, Fang S (2006) Ubiquitin ligase gp78 increases solubility and facilitates degradation of the Z variant of alpha-1-antitrypsin. *Biochem Biophys Res Commun* 349:1285–1293. <https://doi.org/10.1016/j.bbrc.2006.08.173>
 53. Stein A, Ruggiano A, Carvalho P, Rapoport TA (2014) Key steps in ERAD of luminal ER proteins reconstituted with purified components. *Cell* 158:1375–1388. <https://doi.org/10.1016/j.cell.2014.07.050>
 54. Stoller JK, Aboussouan LS (2012) A review of $\alpha 1$ -antitrypsin deficiency. *Am J Respir Crit Care Med* 185:246–259. <https://doi.org/10.1164/rccm.201108-1428CI>
 55. Teckman JH, Burrows J, Hidvegi T et al (2001) The proteasome participates in degradation of mutant alpha 1-antitrypsin Z in the endoplasmic reticulum of hepatoma-derived hepatocytes. *J Biol Chem* 276:44865–44872. <https://doi.org/10.1074/jbc.M103703200>
 56. Toivola DM, Krishnan S, Binder HJ et al (2004) Keratins modulate colonocyte electrolyte transport via protein mistargeting. *J Cell Biol* 164:911–921. <https://doi.org/10.1083/jcb.200308103>
 57. Toivola DM, Strnad P, Habtezion A, Omary MB (2010) Intermediate filaments take the heat as stress proteins. *Trends Cell Biol* 20:79–91. <https://doi.org/10.1016/j.tcb.2009.11.004>
 58. Valley HC, Bukis KM, Bell A, Cheng Y, Wong E, Jordan NJ, Allaire NE, Sivachenko A, Liang F, Bihler H, Thomas PJ, Mahiou J, Mense M (2019) Isogenic cell models of cystic fibrosis-causing variants in natively expressing pulmonary epithelial cells. *J Cyst Fibros* 18(4):476–483. <https://doi.org/10.1016/j.jcf.2018.12.001> (Epub 2018 Dec 15 PMID: 30563749)
 59. van't Wout EFA, Dickens JA, van Schadewijk A et al (2014) Increased ERK signalling promotes inflammatory signalling in primary airway epithelial cells expressing Z $\alpha 1$ -antitrypsin. *Hum Mol Genet* 23:929–941. <https://doi.org/10.1093/hmg/ddt487>
 60. Varga K, Jurkuvenaite A, Wakefield J et al (2004) Efficient intracellular processing of the endogenous cystic fibrosis transmembrane conductance regulator in epithelial cell lines. *J Biol Chem* 279:22578–22584. <https://doi.org/10.1074/jbc.M401522000>
 61. Vasic V, Denkert N, Schmidt CC et al (2020) Hrd1 forms the retrotranslocation pore regulated by auto-ubiquitination and binding of misfolded proteins. *Nat Cell Biol* 22:274–281. <https://doi.org/10.1038/s41556-020-0473-4>
 62. Vitale M, Bakunts A, Orsi A et al (2019) Inadequate BiP availability defines endoplasmic reticulum stress. *Elife*. <https://doi.org/10.7554/eLife.41168>
 63. Wang H, Li Q, Shen Y, et al (2011) The ubiquitin ligase Hrd1 promotes degradation of the Z variant alpha 1-antitrypsin and increases its solubility. *Mol Cell Biochem* 346:137–145. <https://doi.org/10.1007/s11010-010-0600-9>
 64. Wu T, Zhang S, Xu J et al (2020) HRD1, an important player in pancreatic β -cell failure and therapeutic target for type 2 diabetic mice. *Diabetes* 69:940–953. <https://doi.org/10.2337/db19-1060>
 65. Yagishita N, Aratani S, Leach C et al (2012) RING-finger type E3 ubiquitin ligase inhibitors as novel candidates for the treatment of rheumatoid arthritis. *Int J Mol Med* 30:1281–1286. <https://doi.org/10.3892/ijmm.2012.1129>

66. Ye Y, Shibata Y, Yun C, Ron D, Rapoport TA (2004) A membrane protein complex mediates retro-translocation from the ER lumen into the cytosol. *Nature* 429(6994):841–847. <https://doi.org/10.1038/nature02656>. (PMID: 15215856)

Springer Nature or its licensor holds exclusive rights to this article under a publishing agreement with the author(s) or other rightsholder(s); author self-archiving of the accepted manuscript version of this article is solely governed by the terms of such publishing agreement and applicable law.

Publisher's Note Springer Nature remains neutral with regard to jurisdictional claims in published maps and institutional affiliations.

Authors and Affiliations

Iwona Maria Pranke¹ · Benoit Chevalier¹ · Aiswarya Premchandrar³ · Nesrine Baatallah¹ · Kamil F. Tomaszewski¹ · Sara Bitam¹ · Danielle Tondelier¹ · Anita Golec¹ · Jan Stolk⁴ · Gergely L. Lukacs^{5,6} · Pieter S. Hiemstra⁴ · Michal Dadlez³ · David A. Lomas⁷ · James A. Irving⁷ · Agnes Delaunay-Moisant⁸ · Eelco van Anken⁹ · Alexandre Hinzpeter¹ · Isabelle Sermet-Gaudelus^{1,2} · Aleksander Edelman¹ 

¹ Inserm, U1151, CNRS UMR 8253, Université de Paris, 160 rue de Vaugirard, 75015 Paris, France

² Cystic Fibrosis Center, Hôpital Necker Enfants Malades, Assistance Publique Hôpitaux de Paris, Paris, France

³ Laboratory of Mass Spectrometry, Institute of Biochemistry and Biophysics, Polish Academy of Sciences, 02106 Warsaw, Poland

⁴ Department of Pulmonology, Leiden University Medical Center, Leiden, The Netherlands

⁵ Department of Physiology, McGill University, Montréal, QC, Canada

⁶ Department of Biochemistry, McGill University, Montréal, QC, Canada

⁷ UCL Respiratory and the Institute of Structural and Molecular Biology, University College London, London WC1E 6JF, UK

⁸ Institute for Integrative Biology of the Cell (I2BC), Université Paris-Saclay, CEA, CNRS, Gif-sur-Yvette, France

⁹ Division of Genetics and Cell Biology, San Raffaele Scientific Institute, Milan, Italy